An improved combined heat and power economic dispatch model for natural gas combined cycle power plants

Haiquan Yu[1, 2], Lars O. Nord [2], Cong Yu[3], Jianxin Zhou [1], Fengqi Si[1, *]

[1] Key Laboratory of Energy Thermal Conversion and Control of Ministry of Education, School of Energy and Environment, Southeast University, Nanjing, 210096, P.R. China

[2] Department of Energy and Process Engineering, Norwegian University of Science and Technology - NTNU, Trondheim, Norway

[3] Key Laboratory of industrial soot pollution control in Hubei Province, School of Chemistry and Environmental Engineering, Jianghan University, Wuhan, 430056, P.R. China

Corresponding author at:

E-mail addresses: fqsi@seu.edu.cn (Prof. Dr. Fengqi Si), yhq@seu.edu.cn (Haiquan Yu)

Address: School of Energy & Environment, Southeast University, No.2 Sipailou Road, Nanjing, 210096, China.

Tel: +86 25 83790579.

ABSTRACT

An increasing number of natural gas combined cycle (NGCC) plants are operated under combined heat and power mode. Therefore, a combined heat and power economic dispatch (CHPED) is the key to achieve the optimal utilization of fuel. In this paper, an improved CHPED model is developed, in which short-term loads variation process models of plants are integrated to ensure the feasibility of dispatched demands. The short-term loads variation process of NGCC plants is modelled based on the power and heat loads control logic in the field operation process. In comparison with the CHPED models in most existing researches, the improved CHPED model can be applied in the real-time field operation of plants. In addition, the influence of heat load ramp rates on CHPED results is investigated, which can offer theoretical support and guidance for field operation. Based on the data from field operation and manufacturer of an NGCC power station, case studies are performed. Results show that the errors between the short-term loads variation process model and field operational data are less than 2.6 seconds on power load, and less than 1 second on heat load, which proves the accuracy of the model. All the dispatched demands of the improved CHPED model can be met in the required regulation time limits. On one-hour cumulative fuel consumption, the improved CHPED model saves 171.4 kg (0.12%) over the field operational demands. The improved CHPED model not only enhances the economic performance, but also guarantees the operational reliability of plants.

Keywords: Short-term loads variation process; Real-time operation optimization; Heat load ramp rates; Natural gas combined cycle (NGCC); Combined cycle gas turbine (CCGT)

1. Introduction

1.1 Background

Among thermal energy conversion technologies for high power output, natural gas combined cycle (NGCC) power plants are recognized as the most efficient technology to satisfy the growing demand for energy [1]. They are expected to play a crucial role in the future energy portfolio with an increasingly large share of intermittent renewables, due to their high operational flexibility [2, 3]. Currently, the power generation capacity of NGCC plants accounts for more than 20% of the global power generation [4]. By making full use of the heat wasted during power generation, combined heat and power (CHP) plants are able to achieve nearly 90% fuel utilization efficiency, and reduce gas emission by 13–18% [5, 6]. In the context that more and more NGCC plants have been operated under CHP mode [7], the combined heat and power economic dispatch (CHPED) is the key to achieve the optimal utilization of fuel while satisfying demands from power grid and district heating (DH) system [8, 9].

The researches on dealing with economic dispatch (ED) problems in NGCC plants can be categorized into two groups based on the major contributions, including (a) considering more operational factors into ED models, and (b) utilizing new optimization methods to obtain the minimum operational cost. For the first group, in order to more accurately formulate the operation of plants under the current and future energy market, many operational factors have been modelled and integrated into ED models as constraints and cost functions. Heredia et al. [10] and Rist et al. [11] included the cost of start-up and shut-down of plants in the cost function of ED model. In [12-14] different operation states of a plant, and the transition constraints between these states are considered into the ED model. In [15-17], the influence of economic and emission factors on ED calculation results was investigated. Álvarez et al. [18] calculated the cost of curtailing load from interruptible

loads, such as wind and solar power, as a part of the total cost. The energy utilization efficiency models were developed using the field data of plants in Santos's work [19]. For the second group, the researches mainly focused on applying some novel optimization algorithms or strategies to solve the ED problem in NGCC plants, including: particle swarm optimization (PSO) algorithm with circulating the prey technique [20], the combination of surrogate Lagrangian relaxation and branch-and-cut [21, 22], and cuckoo search algorithm [23].

However, in most of the above studies only the power demand was dispatched, without taking the heat demand into account. Although the CHPED problem in NGCC plants was calculated in the researches [11, 17, 19], the NGCC plants in them were not equipped with steam turbine, which means all the steam generated in heat recovery steam generators (HRSG) was led to DH system. The operational characteristics of an NGCC plant with and without steam turbine are quite different. From the perspective of CHPED problems, there are mainly two differences: one is the loads variation characteristic, another is the feasible operating zone (FOZ). A) for an NGCC plant with steam turbine, the power load is the sum of gas turbine output and steam turbine output. The loads variation process of the plant is more complex, which will be presented in detail in this study. B) the FOZ of the plant without steam turbine is a line, which indicates power load and heat load have a one-to-one correspondence. There is no adjustment space for heat load (power load), when power load (heat load) is set. The FOZ of the plant with steam turbine is one or several polygons. There is a certain adjustment space for heat load (power load) under any power load (heat load). The above two characteristics of an NGCC plant with steam turbine make the CHPED problem more complicated.

On the CHPED problem in thermal power plants, many researchers have proposed and improved heuristic optimization algorithms for better searching and convergence performance. Haghrah et al. [24] presented a real coded genetic algorithm with improved Mühlenbein mutation for solving CHPED optimization task. Beigvand et al. [25] carried out some enhancement on PSO algorithm and proposed a novel optimization algorithm called hybrid Time Varying Acceleration Coefficients-Gravitational Search Algorithm. Huang et al. [26] developed a heterogeneous evolving cuckoo search algorithm with a novel constraint-handling mechanism. Zou et al. [27] handled the CHPED problems by an improved genetic algorithm using novel crossover and mutation. Basu et al. [28] employed squirrel search algorithm for solving intricate multi-region CHPED problem with integration of renewable energy.

Furthermore, in some researches the ramp rates of plants were integrated into the CHPED model to achieve the minimum total cost over a short period. In [29-31], the thermal inertia of DH systems and buildings were modelled and employed to minimize the cumulative operational cost of a CHP system. In [32, 33], the influence of extraction-condensing and backpressure modes of CHP plants on CHPED calculation results with multi-objective of profit and emission was examined. Li et al. [34] proposed a CHPED model for the CHP system with thermal energy storage and wind power, considering the cost of emission, incentive cost of demand response, and cost of wind curtailment. Kaur et al. [35] applied the grey wolf optimization algorithm with mutation strategies to solve the CHPED problem of a CHP system incorporating hydro plants. Lahdelma et al. [36] proposed a specialized-power-simplex algorithm to improve the computation efficiency. Bischi et al. [37] presented a CHPED model for the integrated energy system with heat pumps and boilers, considering the electricity price, tariff and cost of start-up and maintenance. Elsido et al. [38] utilized two-stage optimization algorithm to tackle the MINLP calculation of the CHPED problem.

However, the CHPED models in the above researches were mainly established from the perspective of power grid or DH system. Many simplifications and assumptions on the characteristics models of the CHP

plants were made. For instance, the power load ramp rates of plants were set to be a fixed value, or even not taken into account. In the field operation of a CHP plant, there are strongly mutual dependencies between heat generation process and power generation process [39, 40]. The heat load variation process greatly affects the power load ramp rate [41-43]. Especially for an NGCC plant, the power load is the sum of gas turbine output and steam turbine output. The loads variation process of the plant is more complicated. Therefore, in the above researches the formulations of practical loads variation capacity of CHP plants were not accurate enough. It may lead to a too large difference between the dispatched demand and current load of the NGCC plant, so that the dispatched demand cannot be reached in time, which has been proved in the case studies in Section 4 of this paper. If the demands from the power grid and DH system cannot be met in the required time limits, the balance between generation and demand will be broken, which is harmful to the operational reliability and security. For the power plant and station, the priority of the operational reliability and security is the highest.

Besides, to the best of the authors' knowledge, the cost function of a CHP plant in the CHPED models in most existing researches is a quadratic function of power load and heat load. This is because the CHP plants are coal-fired in most of the above studies. Nevertheless, the operational characteristics of an NGCC plant are significantly influenced by ambient temperature [44, 45]. The calculation deviation caused by the cost function without taking the ambient temperature into consideration is even larger than the benefits from CHPED in some cases.

1.2 Research challenge and contribution

Due to the insufficient accuracy of CHP operation process models of NGCC plants, the CHPED models in most existing researches cannot be applied in the real-time field operation. In order to fill the research gap, this study aims to present an improved CHPED model with feasible dispatched demands for NGCC plants that can be directly applied in the real-time field operation. A short-term loads variation process model is developed to quantify the practical loads variation capacity of NGCC plants. The improved CHPED model will help the industry benefit from the significantly lower cost while guarantees the operational reliability of plants. The main contributions of this study are as follows:

(1) A short-term loads variation process model of NGCC plants suitable for the CHPED calculation is developed. Based on the power and heat loads control logic in the field operation process, the model is refined with a rational simplification. As a consequence, the complicated differential equations are avoided to reduce the computation burden of the CHPED model. The accuracy and applicability of the short-term loads variation process model are proved with the field operational data.

(2) An improved CHPED model is proposed with consideration on the field operational characteristics of NGCC plants in detail. The short-term loads variation process model is integrated into the CHPED model to ensure the feasibility of dispatched demands. In comparison with the CHPED models in most existing researches, the improved CHPED model can be applied in the real-time field operation of plants. It can offer guidance for the field operation process as a real-time optimization tool.

(3) The influence rules and reasons of heat load ramp rates on CHPED results are investigated. The influence rules are analyzed and supported from the perspective of the principle of the optimization algorithm. The conclusions can provide theoretical reference for the field operation of plants on heat load ramp rates adjustment.

This paper is structured as follows. Section 2 presents the short-term loads variation process model and the improved CHPED model for NGCC plants. Based on the data from field operation and manufacturer of

an NGCC power station, the plants parameters used in the case studies are set in Section 3. In Section 4 calculation result of the improved CHPED model is compared to that of the regular CHPED model, and the field operational demands. The benefits and effectiveness of the improved CHPED model are demonstrated. Moreover, the influence of heat load ramp rates of plants on CHPED results is investigated. Conclusions are given in Section 5.

2. Methodology

2.1 Short-term loads variation process model of NGCC plants

2.1.1 Heat and power loads variation process model

Two common configurations of NGCC plants are shown in Fig. 1. The 1×1 plant comprises a gas turbine with the corresponding HRSG and a steam turbine. The 2×1 plant comprises two gas turbines with the corresponding HRSGs and a steam turbine. Partial steam is extracted from steam turbines as the heat source of DH system. As an initial condition, the time when a plant receives new heat and power demands is t_0. The actual heat load and power load of the plant at that time are represented as $Q(t_0)$ and $P(t_0)$ respectively. The new heat demand and power demand are represented as $Q_D(t_0)$ and $P_D(t_0)$ respectively. After that, the flow of extracted process steam and the gas turbine output are regulated immediately. At the time of t_1, the heat load of the plant ($Q(t_1)$) can be calculated as

$$Q(t_1)=\begin{cases} Q(t_0)+\alpha\int_{t_0}^{t_1} R_H(t)\,dt & t_0 \le t_1 \le t_{HS} \\ Q_D(t_0) & t_1 > t_{HS} \end{cases} \tag{1}$$

where t_{HS} is the time when the plant heat load reaches the heat demand. $R_H(t)$ is the plant heat load ramp rate. α is a coefficient indicating the relationship between heat load ($Q(t_0)$) and heat demand ($Q_D(t_0)$) at the time of t_0:

$$\alpha=\begin{cases} 1 & Q(t_0) \le Q_D(t_0) \\ -1 & Q(t_0) > Q_D(t_0) \end{cases} \tag{2}$$

At the time of t_1, the power load of the plant ($P(t_1)$) can be calculated as

$$P(t_1)=\begin{cases} P(t_0)+\int_{t_0}^{t_1} R_P(t)\,dt & t_0 \le t_1 \le t_{PS} \\ P_D(t_0) & t_1 > t_{PS} \end{cases} \tag{3}$$

where t_{PS} is the time when the plant power load reaches the power demand. $R_P(t)$ is the plant power load ramp rate, determined by the output variation rates of gas turbine ($R_{GT}(t)$) and steam turbine ($R_{ST}(t)$):

$$R_P(t)=\beta(t)\cdot R_{GT}(t)+R_{ST}(t) \tag{4}$$

$$R_{GT}(t)=\sum_{i=1}^{I} R_{GT,i}(t) \tag{5}$$

where I is the amount of gas turbines in the plant, which equals to 1 for the 1×1 plant and equals to 2 for the 2×1 plant. $\beta(t)$ is a coefficient indicating the relationship between the current plant power load ($P(t)$) and

power demand ($P_D(t_0)$):

$$\beta(t)=\begin{cases}1 & P(t)\le P_D(t_0)\\ -1 & P(t)>P_D(t_0)\end{cases} \tag{6}$$

The steam turbine output in an NGCC plant is mainly determined by the live steam parameters of each water-steam circuit and the heat load (Q). The live steam parameters are mainly determined by the inlet gas temperature and mass flow of HRSG, which are the function of gas turbine output (P_{GT}) and ambient temperature (T_A). The above relationship can be organized as:

$$P_{ST}=f(P_{GT},T_A,Q) \tag{7}$$

Therefore, at a given ambient temperature, the output variation rate of steam turbine ($R_{ST}(t)$) can be calculated as:

$$R_{ST}(t)=\beta(t-\Delta t_{DE})\cdot R_{ST}^{GT}(t)+(-\alpha)\cdot R_{ST}^{H}(t) \tag{8}$$

where $R_{ST}^{GT}(t)$ and $R_{ST}^{H}(t)$ are output variation rates of the steam turbine caused by the changes of gas turbine output and heat load, respectively. Due to the slow heat exchange processes in HRSG, after the change of gas turbine output, there is a certain time delay before the corresponding variation of steam turbine output in the continuous operation process [46-48]. The time delay is represented as Δt_{DE}. Thus, the $R_{ST}^{GT}(t)$ is caused by the $R_{GT}(t-\Delta t_{DE})$, rather than $R_{GT}(t)$. And the direction of $R_{ST}^{GT}(t)$ is the same as the change direction of gas turbine output at the time of $(t-\Delta t_{DE})$, i.e. $\beta(t-\Delta t_{DE})$. The heat load and steam turbine output are negatively correlated. If the flow of extracted process steam increases, the heat load will rise and steam turbine output will drop. If the flow of extracted process steam decreases, the heat load will drop and steam turbine output will rise. As the heat load control is achieved directly by adjusting the flow valve of extracted process steam, there is almost no delay for the resulting variation of steam turbine output. Consequently, in Eq. (8), the negative α is used to express the direction of $R_{ST}^{H}(t)$.

On the basis of Eq. (7), a coefficient is defined to indicate the variation of steam turbine output caused by each unit of heat load:

$$\theta_{ST}^{H}=\left.\frac{\partial P_{ST}(Q)}{\partial Q}\right|_{\substack{P_{GT}=\text{const}\\ T_A=\text{const}}} \tag{9}$$

where θ_{ST}^{H} is insensitive to time (t), but related with gas turbine output (P_{GT}) and ambient temperature (T_A), theoretically. The θ_{ST}^{H} under different operating conditions can be obtained through simulation, and the output variation rate of steam turbine caused by the heat load change can be written as:

$$R_{ST}^{H}(t)=\theta_{ST}^{H}\cdot R_{H}(t) \tag{10}$$

Substituting Eq. (8) ~ (10) into Eq. (4), then the plant power load ramp rate ($R_P(t)$) can be expressed as

$$R_P(t)=\beta(t)\cdot R_{GT}(t)+R_{ST}(t)=\beta(t)\cdot R_{GT}(t)+\beta(t-\Delta t_{DE})\cdot R_{ST}^{GT}(t)+(-\alpha)\cdot\theta_{ST}^{H}\cdot R_{H}(t) \tag{11}$$

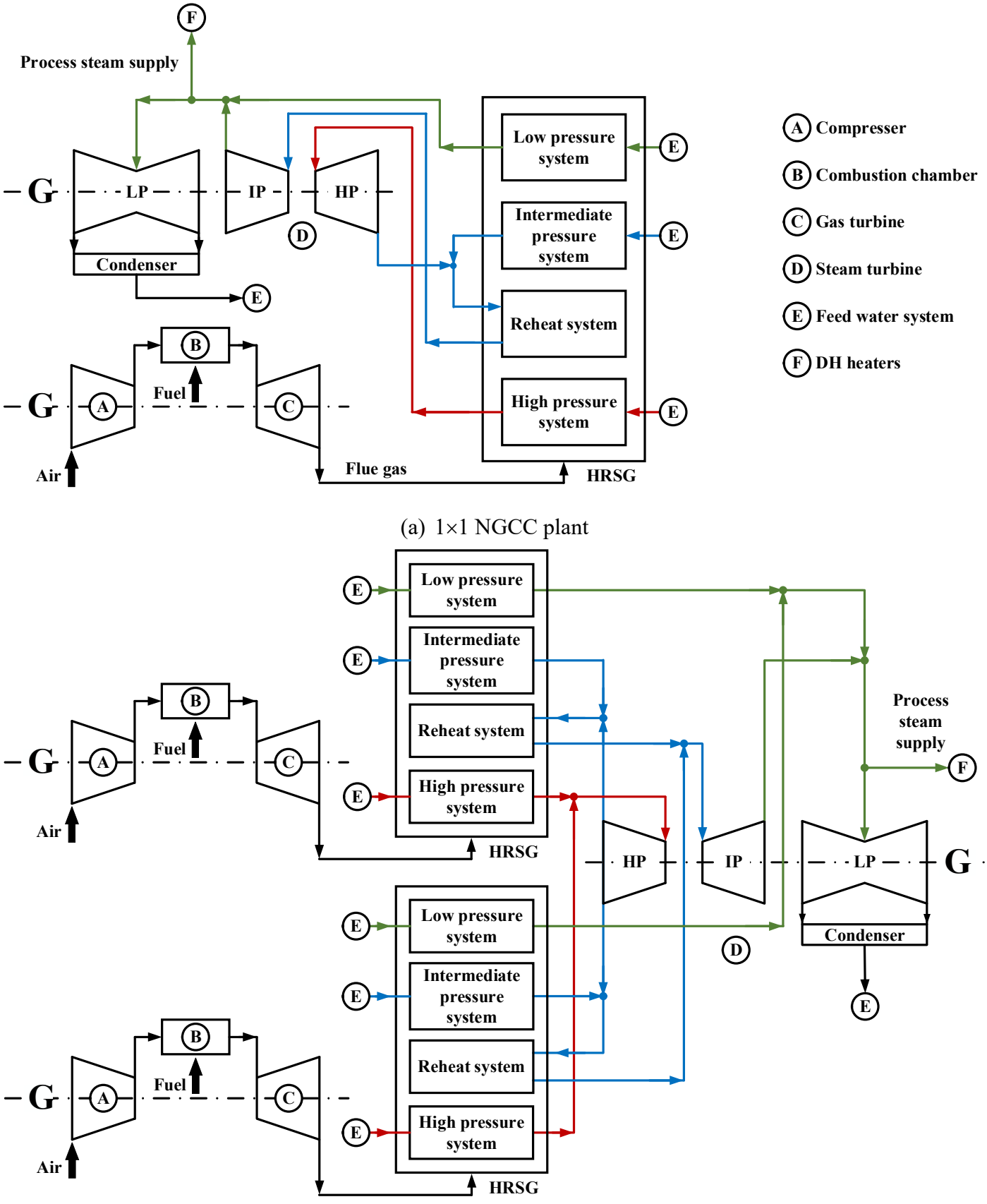

(a) 1×1 NGCC plant

(b) 2×1 NGCC plant

Fig. 1. Schematic diagram of 1×1 and 2×1 NGCC plants at CHP mode.

2.1.2 *Short-term loads variation process model*

As mentioned above, in the continuous operation process of an NGCC plant, after the change of gas turbine output, there is a certain time delay before the corresponding variation of steam turbine output. Moreover, the output variation rate of steam turbine is much smaller than that of gas turbine. Therefore, in order to meet the power demand as soon as possible, the field control logic on power load of an NGCC plant under load following mode is generally: after a new power demand is received, firstly, the gas turbine output is adjusted to make the plant power load meet the demand. After several minutes, the steam turbine output gradually changes with the variation of live steam parameters. In the meanwhile, the gas turbine output is adjusted with the change of steam turbine output to maintain the balance between power load and demand of the plant. In the control circuit of gas turbine, the output set-value is the difference between the power demand and current steam turbine output.

At CHP mode, the heat load control is achieved directly by adjusting the valve opening of extracted process steam pipeline. Due to the rapid action of flow valve, the heat load ramp rate is relatively large. Consequently, in comparison to the variation of steam turbine output caused by the gas turbine output change, the variation caused by the heat load change has the following two characteristics: a) the delay is small enough to be negligible; b) the variation rate is much larger. In this study, the "short-term" refers to the time interval between two demands, which is usually less 3 minutes under various demands scenarios. Based on the analysis above, for the short-term loads variation process model, two assumptions are made as follows, of which the rationality is validated in Section 4.1:

(1) Since the output variation rate of steam turbine caused by gas turbine is much smaller than that of gas turbine, in the field power load adjustment process, the output variation of steam turbine caused by gas turbine can be rapidly balanced by gas turbine. Therefore, for the short-term power load variation process, it is assumed that only the influence of heat load change is considered in the calculation of the output variation rate of steam turbine, and the influence of gas turbine output change is neglected. In addition, the influence of gas turbine is calculated based on the gas turbine output variation process in several previous demand periods. It will greatly increase the computation burden of CHPED model. It should be noted that this assumption is made on the basis of the field control logic on power load of an NGCC plant under load following mode, and only suitable for the short-term power load variation process. As a consequence, Eq. (8) is simplified as:

$$R_{\mathrm{ST}}(t) = (-\alpha) \cdot R_{\mathrm{ST}}^{\mathrm{H}}(t) \tag{12}$$

(2) In general, the variation rate of the extracted process steam flow is insensitive to time [41], which means $R_{\mathrm{H}}(t) = R_{\mathrm{H}}$. It is assumed that in the short-term, the output variation rate of gas turbine is a constant value, which means $R_{\mathrm{GT}}(t) = R_{\mathrm{GT}}$. As a consequence, Eq. (11) is simplified as:

$$R_{\mathrm{P}}(t) = \beta(t) \cdot R_{\mathrm{GT}} + (-\alpha) \cdot \theta_{\mathrm{ST}}^{\mathrm{H}} \cdot R_{\mathrm{H}} \tag{13}$$

In the short-term loads variation process model, the required adjustment amounts of heat load (ΔQ) and power load (ΔP) of the plant are defined as:

$$\Delta Q = \left| Q_{\mathrm{D}}(t_0) - Q(t_0) \right| \tag{14}$$

$$\Delta P = \left| P_{\mathrm{D}}(t_0) - P(t_0) \right| \tag{15}$$

Based on the two assumptions above, the time when plant heat load reaches the demand (t_{HS}), and the heat load at the time of t_1 ($Q(t_1)$) are calculated as:

$$t_{HS} = t_0 + \frac{\Delta Q}{R_H} \tag{16}$$

$$Q(t_1) = \begin{cases} Q(t_0) + \alpha \cdot R_H \cdot (t_1 - t_0) & t_0 \le t_1 \le t_{HS} \\ Q_D(t_0) & t_1 > t_{HS} \end{cases} \tag{17}$$

The model of plant power load variation process in short-term can be described as the following six scenarios (S1~S6), based on the required variation direction of plant heat load (α), the required variation direction of plant power load ($\beta(t_0)$), the output variation rate of gas turbine (R_{GT}), and the output variation rate of steam turbine caused by heat load change (R_{ST}^H). The logic diagram of the short-term power load variation process model of an NGCC plant is shown in Fig. 3.

If the required variation directions of plant heat load and power load are the same, i.e. $\alpha \cdot \beta(t_0) = 1$, the variation direction of steam turbine output caused by heat load change will be opposite to that of gas turbine output. There is a negative effect on the satisfaction of power demand. Under this condition, if the output variation rate of gas turbine is larger than that of steam turbine caused by heat load change, i.e. $R_{GT} \ge R_{ST}^H$, the plant power load will continuously approach the power demand. If $R_{GT} < R_{ST}^H$, firstly the plant power load will be away from the power demand before the heat demand is met. Then the power load will approach the power demand after the heat demand is met. The scenarios S1, S2 and S3 are as follows:

Scenario S1: ($\alpha \cdot \beta(t_0) = 1$) & ($R_{GT} \ge R_{ST}^H$) & ($\frac{\Delta P}{R_{GT} - R_{ST}^H} \le t_{HS}$). In this situation, the power demand will be met earlier than heat demand, and the plant power load ramp rate will be ($R_{GT} - R_{ST}^H$). The time when the plant power load reaches the demand (t_{PS}) is calculated as Eq. (18). The plant power load at the time of t_1 ($P(t_1)$) is calculated as Eq. (19). The corresponding schematic diagram of the plant power load variation process is shown in Fig. 2(a).

$$t_{PS} = t_0 + \frac{\Delta P}{R_{GT} - R_{ST}^H} \tag{18}$$

$$P(t_1) = \begin{cases} P(t_0) + \beta(t_0) \cdot (R_{GT} - R_{ST}^H) \cdot (t_1 - t_0) & t_0 \le t_1 \le t_{PS} \\ P_D(t_0) & t_1 > t_{PS} \end{cases} \tag{19}$$

Scenario S2: ($\alpha \cdot \beta(t_0) = 1$) & ($R_{GT} \ge R_{ST}^H$) & ($\frac{\Delta P}{R_{GT} - R_{ST}^H} > t_{HS}$). In this situation, the heat demand will be met earlier than power demand. The plant power load ramp rate will increase from ($R_{GT} - R_{ST}^H$) to R_{GT}, after the heat demand is met. The t_{PS} and $P(t_1)$ are calculated as Eq. (20) and Eq. (21). The corresponding schematic diagram of the plant power load variation process is shown in Fig. 2(b).

$$t_{PS} = t_{HS} + \frac{\Delta P - (R_{GT} - R_{ST}^H) \cdot (t_{HS} - t_0)}{R_{GT}} \tag{20}$$

$$P(t_1)=\begin{cases} P(t_0)+\beta(t_0)\cdot\left(R_{GT}-R_{ST}^{H}\right)\cdot(t_1-t_0) & t_0\le t_1\le t_{HS} \\ P(t_0)+\beta(t_0)\cdot\left(R_{GT}-R_{ST}^{H}\right)\cdot(t_{HS}-t_0)+\beta(t_0)\cdot R_{GT}\cdot(t_1-t_{HS}) & t_{HS}<t_1\le t_{PS} \\ P_D(t_0) & t_1>t_{PS} \end{cases} \tag{21}$$

Scenario S3: ($\alpha\cdot\beta(t_0)=1$) & ($R_{GT}<R_{ST}^{H}$). In this situation, firstly the plant power load will be away from the power demand at a rate of ($R_{ST}^{H}-R_{GT}$), before the heat demand is met. Then the power load will approach the power demand at a rate of R_{GT}, after the heat demand is met. The t_{PS} and $P(t_1)$ are calculated as Eq. (22) and Eq. (23). The corresponding schematic diagram of the plant power load variation process is shown in Fig. 2(c).

$$t_{PS}=t_{HS}+\frac{\Delta P+\left(R_{ST}^{H}-R_{GT}\right)\cdot(t_{HS}-t_0)}{R_{GT}} \tag{22}$$

$$P(t_1)=\begin{cases} P(t_0)-\beta(t_0)\cdot\left(R_{ST}^{H}-R_{GT}\right)\cdot(t_1-t_0) & t_0\le t_1\le t_{HS} \\ P(t_0)-\beta(t_0)\cdot\left(R_{ST}^{H}-R_{GT}\right)\cdot(t_{HS}-t_0)+\beta(t_0)\cdot R_{GT}\cdot(t_1-t_{HS}) & t_{HS}<t_1\le t_{PS} \\ P_D(t_0) & t_1>t_{PS} \end{cases} \tag{23}$$

If the required variation directions of plant heat load and power load are opposite, i.e. $\alpha\cdot\beta(t_0)=-1$, the variation direction of steam turbine output caused by heat load change will be the same with that of gas turbine output. Under this condition, if $\frac{\Delta P}{R_{GT}+R_{ST}^{H}}\le t_{HS}$, the power demand will be met earlier, otherwise, the heat demand will be met earlier. The scenarios S4, S5 and S6 are as follows:

Scenario S4: ($\alpha\cdot\beta(t_0)=-1$) & ($\frac{\Delta P}{R_{GT}+R_{ST}^{H}}\le t_{HS}$) & ($R_{GT}\ge R_{ST}^{H}$). In this situation, the plant power load ramp rate will be ($R_{GT}+R_{ST}^{H}$). The t_{PS} and $P(t_1)$ are calculated as Eq. (24) and Eq. (25). The corresponding schematic diagram of the plant power load variation process is shown in Fig. 2(d).

$$t_{PS}=t_0+\frac{\Delta P}{R_{GT}+R_{ST}^{H}} \tag{24}$$

$$P(t_1)=\begin{cases} P(t_0)+\beta(t_0)\cdot\left(R_{GT}+R_{ST}^{H}\right)\cdot(t_1-t_0) & t_0\le t_1\le t_{PS} \\ P_D(t_0) & t_1>t_{PS} \end{cases} \tag{25}$$

Scenario S5: ($\alpha\cdot\beta(t_0)=-1$) & ($\frac{\Delta P}{R_{GT}+R_{ST}^{H}}\le t_{HS}$) & ($R_{GT}<R_{ST}^{H}$). In this situation, firstly the plant power load will rapidly reach the power demand at a rate of ($R_{GT}+R_{ST}^{H}$), but it is a fake satisfaction of power demand. Then the plant power load will be away from the power demand at a rate of ($R_{ST}^{H}-R_{GT}$), because the steam turbine output is still changing before the heat demand is met. Finally, the plant power load will approach the power demand at a rate of R_{GT}, after the heat demand is met. The t_{PS} and $P(t_1)$ are calculated

as Eq. (26) and Eq. (27). The corresponding schematic diagram of the plant power load variation process is shown in Fig. 2 (e).

$$t_{\mathrm{PS}}=t_{\mathrm{HS}}+\frac{\left(R_{\mathrm{ST}}^{\mathrm{H}}-R_{\mathrm{GT}}\right)\cdot\left(t_{\mathrm{HS}}-t_0-\dfrac{\Delta P}{R_{\mathrm{GT}}+R_{\mathrm{ST}}^{\mathrm{H}}}\right)}{R_{\mathrm{GT}}} \tag{26}$$

$$P\left(t_1\right)=\begin{cases}P\left(t_0\right)+\beta\left(t_0\right)\cdot\left(R_{\mathrm{GT}}+R_{\mathrm{ST}}^{\mathrm{H}}\right)\cdot\left(t_1-t_0\right) & t_0\le t_1\le t_0+\dfrac{\Delta P}{R_{\mathrm{GT}}+R_{\mathrm{ST}}^{\mathrm{H}}}\\ P_{\mathrm{D}}\left(t_0\right)+\beta\left(t_0\right)\cdot\left(R_{\mathrm{ST}}^{\mathrm{H}}-R_{\mathrm{GT}}\right)\cdot\left(t_1-t_0-\dfrac{\Delta P}{R_{\mathrm{GT}}+R_{\mathrm{ST}}^{\mathrm{H}}}\right) & t_0+\dfrac{\Delta P}{R_{\mathrm{GT}}+R_{\mathrm{ST}}^{\mathrm{H}}}<t_1\le t_{\mathrm{HS}}\\ P_{\mathrm{D}}\left(t_0\right)+\beta\left(t_0\right)\cdot\left(R_{\mathrm{ST}}^{\mathrm{H}}-R_{\mathrm{GT}}\right)\cdot\left(t_{\mathrm{HS}}-t_0-\dfrac{\Delta P}{R_{\mathrm{GT}}+R_{\mathrm{ST}}^{\mathrm{H}}}\right)-\beta\left(t_0\right)\cdot R_{\mathrm{GT}}\cdot\left(t_1-t_{\mathrm{HS}}\right) & t_{\mathrm{HS}}<t_1\le t_{\mathrm{PS}}\\ P_{\mathrm{D}}\left(t_0\right) & t_1>t_{\mathrm{PS}}\end{cases} \tag{27}$$

Scenario S6: ($\alpha\cdot\beta(t_0)=-1$) & ($\dfrac{\Delta P}{R_{\mathrm{GT}}+R_{\mathrm{ST}}^{\mathrm{H}}}>t_{\mathrm{HS}}$). In this situation, the heat demand will be met earlier than power demand. The plant power load ramp rate will decrease to R_{GT} from ($R_{\mathrm{GT}}+R_{\mathrm{ST}}^{\mathrm{H}}$), after the heat demand is met. The t_{PS} and $P(t_1)$ are calculated as Eq. (28) and Eq. (29). The corresponding schematic diagram of the plant power load variation process is shown in Fig. 2 (f).

$$t_{\mathrm{PS}}=t_{\mathrm{HS}}+\frac{\Delta P-\left(R_{\mathrm{GT}}+R_{\mathrm{ST}}^{\mathrm{H}}\right)\cdot\left(t_{\mathrm{HS}}-t_0\right)}{R_{\mathrm{GT}}} \tag{28}$$

$$P\left(t_1\right)=\begin{cases}P\left(t_0\right)+\beta\left(t_0\right)\cdot\left(R_{\mathrm{GT}}+R_{\mathrm{ST}}^{\mathrm{H}}\right)\cdot\left(t_1-t_0\right) & t_0\le t_1\le t_{\mathrm{HS}}\\ P\left(t_0\right)+\beta\left(t_0\right)\cdot\left(R_{\mathrm{GT}}+R_{\mathrm{ST}}^{\mathrm{H}}\right)\cdot\left(t_{\mathrm{HS}}-t_0\right)+\beta\left(t_0\right)\cdot R_{\mathrm{GT}}\cdot\left(t_1-t_{\mathrm{HS}}\right) & t_{\mathrm{HS}}<t_1\le t_{\mathrm{PS}}\\ P_{\mathrm{D}}\left(t_0\right) & t_1>t_{\mathrm{PS}}\end{cases} \tag{29}$$

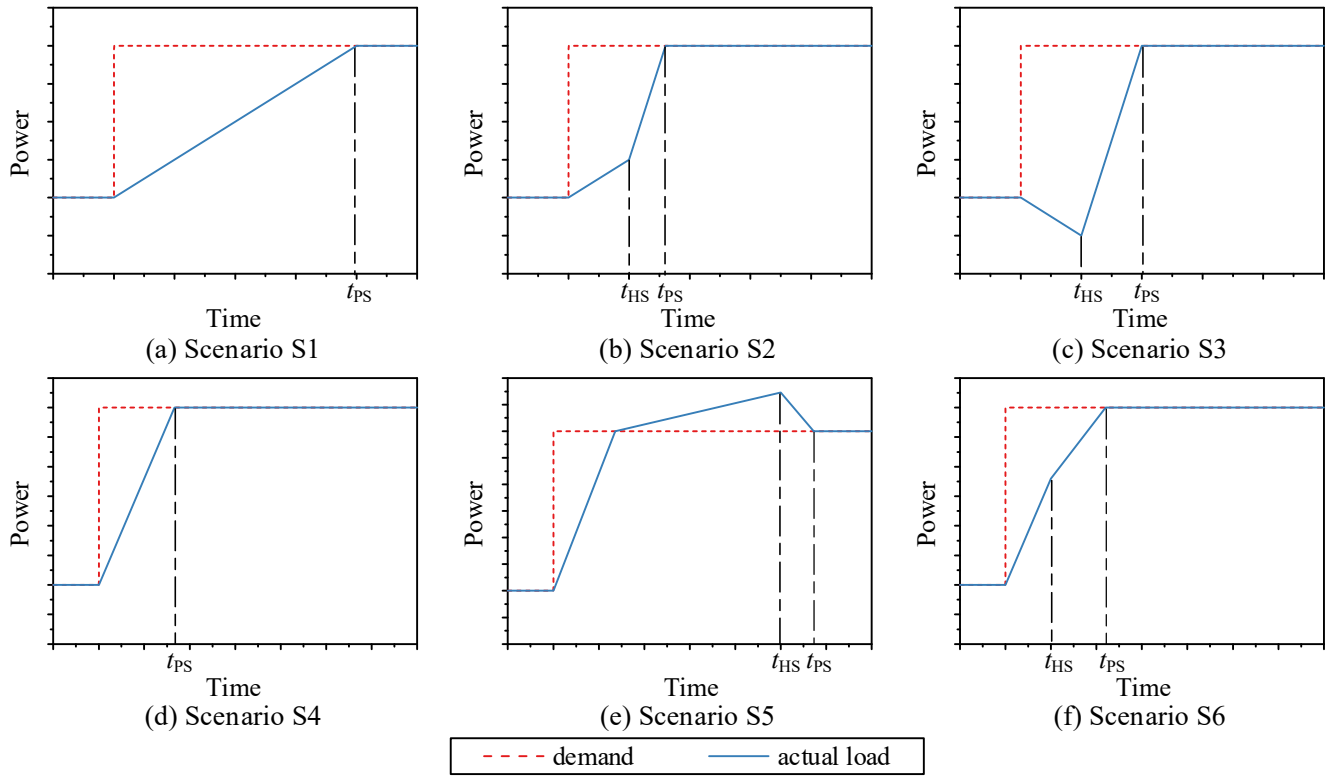

Fig. 2. Schematic diagram of the short-term power load variation process of an NGCC plant.

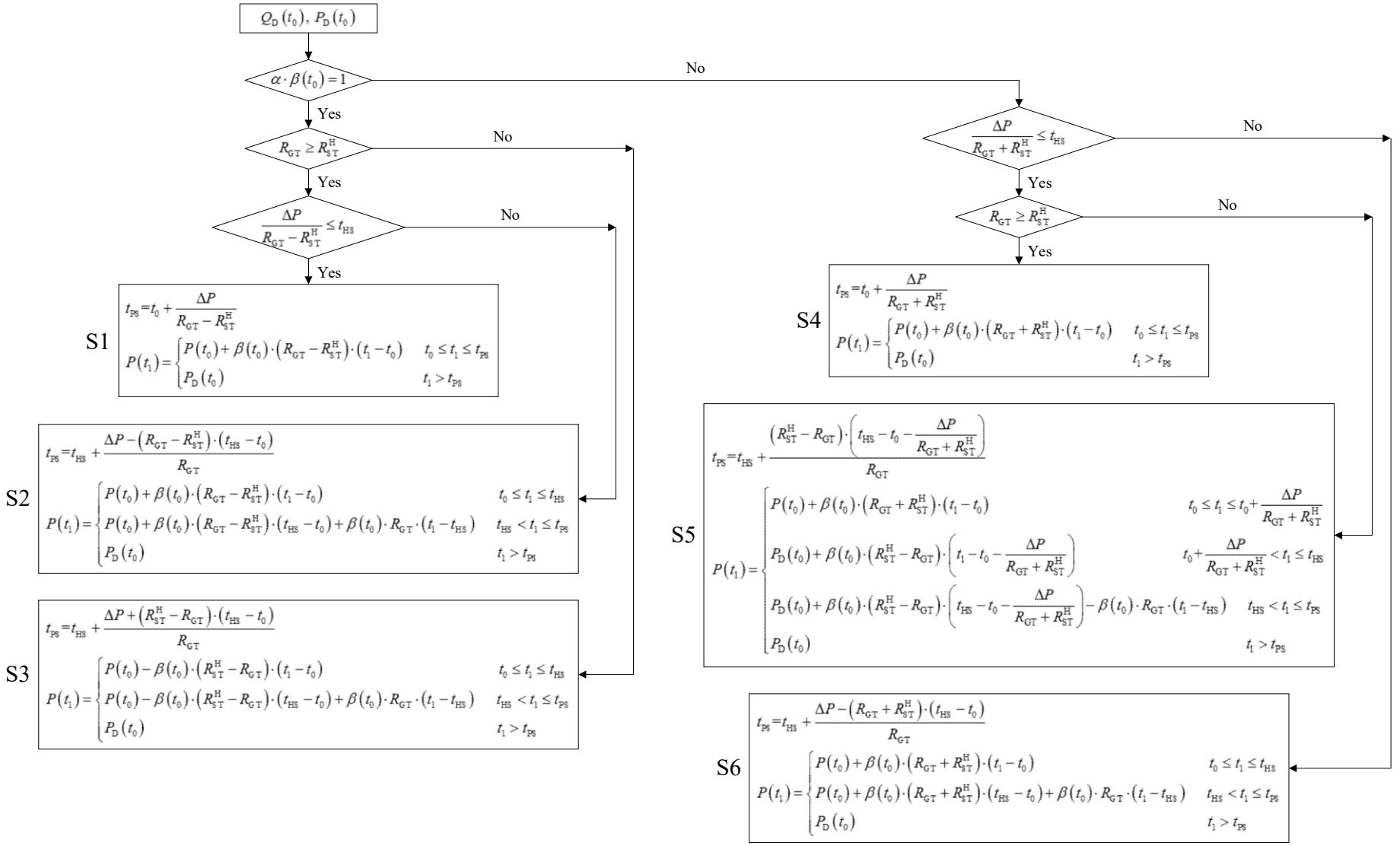

Fig. 3. Logic diagram of the short-term power load variation process model of an NGCC plant.

2.2 The improved CHPED model

The CHPED problem aims to minimize the total operational cost under practical constraints [24-28]. In order to ensure the feasibility of the dispatched heat and power demands, the regular CHPED model is improved in this study. The short-term loads variation process model of each plant is integrated into the improved CHPED model, so that the heat and power demands and actual loads can be distinguished. Mathematical formulations of the improved CHPED model are presented in this section.

As an initial condition, the time when the power station receives new heat and power demands is t_0. The objective function is to determine the heat and power demands of each NGCC plant for achieving the minimum total operational cost, which is defined as:

$$\text{Minimize} \sum_{i=1}^{N} C_i\left(P_{\mathrm{D},i}\left(t_0\right), Q_{\mathrm{D},i}\left(t_0\right), T_{\mathrm{A}}\right) \tag{30}$$

where C_i is the cost function of the ith (i=1, 2, …, N) NGCC plant. $Q_{\mathrm{D},i}(t_0)$ and $P_{\mathrm{D},i}(t_0)$ are the heat and power demands of the ith plant at the time of t_0, respectively.

The total cost minimization task of the CHPED problem should be subjected to the following equality and inequality constraints:

(1) Heat demands balance

$$\sum_{i=1}^{N} Q_{\mathrm{D},i}\left(t_0\right) = Q_{\mathrm{D,DH}}\left(t_0\right) \tag{31}$$

where $Q_{\mathrm{D,DH}}(t_0)$ is the heat demand from DH system at the time of t_0.

(2) Power demands balance

$$\sum_{i=1}^{N} P_{\mathrm{D},i}\left(t_0\right) = P_{\mathrm{D,PG}}\left(t_0\right) \tag{32}$$

where $P_{\mathrm{D,PG}}(t_0)$ is the power demand from power grid at the time of t_0.

(3) Capacity limits of NGCC plants in CHP mode

$$Q_{\mathrm{MIN},i}\left(P_{\mathrm{D},i}\left(t_0\right), T_{\mathrm{A}}\right) \le Q_{\mathrm{D},i}\left(t_0\right) \le Q_{\mathrm{MAX},i}\left(P_{\mathrm{D},i}\left(t_0\right), T_{\mathrm{A}}\right), \quad \forall i \in [1,2,\cdots,N] \tag{33}$$

$$P_{\mathrm{MIN},i}\left(Q_{\mathrm{D},i}\left(t_0\right), T_{\mathrm{A}}\right) \le P_{\mathrm{D},i}\left(t_0\right) \le P_{\mathrm{MAX},i}\left(Q_{\mathrm{D},i}\left(t_0\right), T_{\mathrm{A}}\right), \quad \forall i \in [1,2,\cdots,N] \tag{34}$$

where $Q_{\mathrm{MIN},i}$ and $Q_{\mathrm{MAX},i}$ are the minimum and maximum heat generation capacity functions of the ith NGCC plant. $P_{\mathrm{MIN},i}$ and $P_{\mathrm{MAX},i}$ are the minimum and maximum power generation capacity functions of the ith NGCC plant. The heat and power generation capacities of a plant have a bidirectional interdependence, which is known as the feasible operating zone (FOZ). For an NGCC plant, the FOZ is influenced by the ambient temperature.

(4) Feasibility requirement of demands

For the sake of operational reliability and security of plants, the power and heat demands of each plant should be met within the required regulation time limits.

$$P_i\left(t_0 + \Delta t_{\mathrm{PG}}\right) = P_{\mathrm{D},i}\left(t_0\right), \quad \forall i \in [1,2,\cdots,N] \tag{35}$$

$$Q_i\left(t_0+\Delta t_{\mathrm{DH}}\right)=Q_{\mathrm{D},i}\left(t_0\right),\qquad \forall i\in[1,2,\cdots,N] \tag{36}$$

$$\left[P_i\left(t_0+\Delta t_{\mathrm{PG}}\right),Q_i\left(t_0+\Delta t_{\mathrm{PG}}\right)\right]=f_i\left(P_i\left(t_0\right),Q_i\left(t_0\right),P_{\mathrm{D},i}\left(t_0\right),Q_{\mathrm{D},i}\left(t_0\right),\Delta t_{\mathrm{PG}}\right),\qquad \forall i\in[1,2,\cdots,N] \tag{37}$$

$$\left[P_i\left(t_0+\Delta t_{\mathrm{DH}}\right),Q_i\left(t_0+\Delta t_{\mathrm{DH}}\right)\right]=f_i\left(P_i\left(t_0\right),Q_i\left(t_0\right),P_{\mathrm{D},i}\left(t_0\right),Q_{\mathrm{D},i}\left(t_0\right),\Delta t_{\mathrm{DH}}\right),\qquad \forall i\in[1,2,\cdots,N] \tag{38}$$

where Δt_{PG} and Δt_{DH} are the required regulation time limits from power grid and DH system, respectively. $P_i(t)$ and $Q_i(t)$ are actual power load and heat load of the ith plant at the time of t. f_i represents the short-term loads variation process model of the ith plant.

The comparison between the regular CHPED model in researches [24-28] and the improved CHPED model is shown in Fig. 4. The difference is the constraint (4). In the regular CHPED model, there are only constraints (1-3), but no constraint (4).

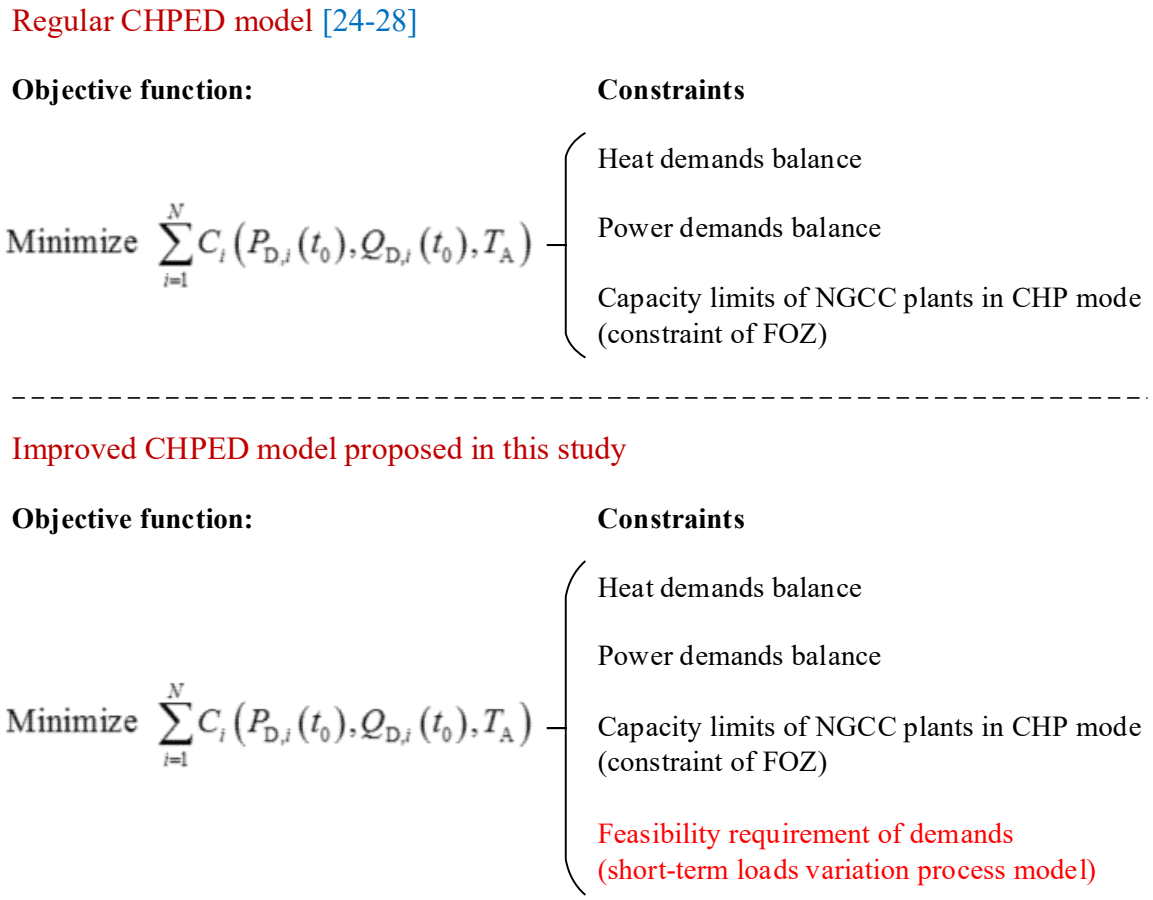

Fig. 4. Comparison between the regular CHPED model [24-28] and the improved CHPED model.

It should be noted that the short-term loads variation process model is developed based on the field loads control logic of an NGCC plant under load following mode. Therefore, the improved CHPED model can be only applied in the real-time field operation of NGCC plants under load following mode. The start-up, shut-down and operation state transition of an NGCC plant are not considered into the improved CHPED model.

2.3 Implementation of CST-PSO algorithm on CHPED problem

In this study, a particle swarm optimization algorithm with chaos searching technique (CST-PSO)

algorithm [49-53] is employed to calculate CHPED models. The optimization variables manipulated by the CST-PSO algorithm are the heat and power demands of each NGCC plant. In the constraints handling process, a novel particle position correction strategy is proposed to improve the calculation efficiency. The detailed process of the implementation of CST-PSO algorithm and particle position correction strategy on the improved CHPED model are illustrated in Section S1 in supplementary material.

3. Case description and simulation

3.1 The reference NGCC power station

In this study, an NGCC power station, which includes one 1×1 plant and one 2×1 plant, is taken as the reference system. The power station is located in North China, and the local ambient temperature annually ranges from 263.15 K to 311.15 K. Every gas turbine in both plants is Siemens SGT5-4000F and equipped with a triple pressure reheat sub-critical HRSG. Two steam turbines are both composed of a high pressure (HP) cylinder, an intermediate pressure (IP) cylinder and a low pressure (LP) cylinder. In each steam turbine, the process steam supplied to DH heaters is extracted from IP cylinder exhaust steam, and the LP exhausted steam is led to a direct water-cooling condenser. The configuration of these two plants is shown in Fig. 1, and the nominal values of technical parameters at design condition are summarized in Table S1. The part-load control strategy of gas turbines is variable inlet guide vane (VIGV) to keep gas turbine exhaust temperature constant. Sliding pressure operation is adopted in the steam turbines. In order to simulate these two plants, thermodynamic models are established with Ebsilon Professional [54], which has been widely used for design, analysis and optimization of various energy system in many researches [55-60]. Details of the modelling methodology are adopted from our previous work [61]. With the help of the thermodynamic models, simulation and study on a wide range of off-design conditions can be performed.

3.2 Basic information of the calculation cases

In order to test the improved CHPED model, one-hour demands are acquired from the field operational data of the power station as a calculation case. There are 56 demands in this one hour, as shown in Fig. 5. During this period, both steam turbines are at extraction-condensing mode in the field operational process, and the ambient temperature increases from 272.75 K to 273.46 K gradually.

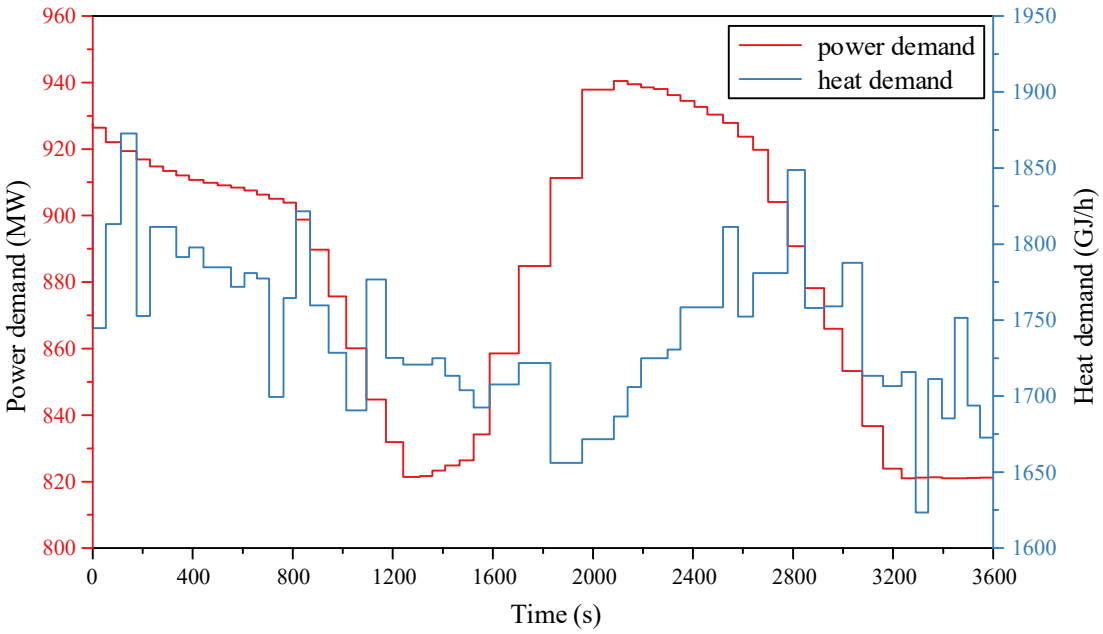

Fig. 5. One-hour demands from field operational data of the power station.

In the operation evaluation documents of the power grid, where the power station in this study is located, the required regulation time limit on power load (Δt_{PG}) is set as Eq. (39). In comparison with the power grid, the requirement from DH system is relatively loose [62]. But for the sake of the operational reliability of DH system, the heat demand should be met before the next demand arrives. Based on the statistical results of the field operational data in the recent half year, the minimum time interval between two demands is 45s. In addition, this time interval must be longer than Δt_{PG}. Therefore, the required regulation time limit on heat load (Δt_{DH}) is set as Eq. (40) in this study.

$$\Delta t_{PG} = \mathrm{MAX}\left\{20\mathrm{s}, \frac{\Delta P}{1\%P_N / \mathrm{min}} \times 60\mathrm{s/min}\right\} \tag{39}$$

$$\Delta t_{DH} = \mathrm{MAX}\left\{45\mathrm{s}, \Delta t_{PG}\right\} \tag{40}$$

The NGCC plant parameters used in the CHPED calculation include: the ramp rate of gas turbine (R_{GT}), the ramp rate of plant heat load (R_H), the coefficient between steam turbine output and heat load (θ_{ST}^H), FOZ and fuel consumption characteristic. Since R_{GT} and R_H are dynamic characteristic parameters, they are set based on the field operational data. θ_{ST}^H, FOZ and fuel consumption characteristic are static characteristic parameters. In contrast with the field operational data, the thermodynamic models can cover a much wider range of off-design conditions. Thus, these three parameters are calculated from the thermodynamic models. Details on each parameter setting are as follows:

(1) R_{GT}

One-hour field operational data of 1×1 plant at condensing mode (non-heat supply) is shown in Fig. 6. It can be seen that the maximum gas turbine output variation rate is approximately 10.5 MW/min. According to the field operating rules documents of the plants in this study, R_{GT} is limited by the thermal stress of HRSG and steam turbine, which is set to be 11 MW/min by operators. The small deviation between historical value and set value may be caused by the storage precision of the field database, which is not high enough. Therefore, R_{GT} of 1×1 plant and 2×1 plant are set to be 11 MW/min

and 22 MW/min in the calculation case, which represents the maximum load variation capacity of the plant in the field operation. If the dispatched demands cannot be met under this scenario, it indicates that they are unfeasible.

(2) R_H

The loads variation process of the 1×1 plant is shown in Fig. 7. The field operational data in the figures shows that heat load ramp rate of 1x1 plant is approximately 71 GJ/(h·min). Based on the field operational data of the 2x1 plant, the heat load ramp rate is approximately 207 GJ/(h·min).

(3) θ_{ST}^{H}

The relationship between steam turbine output and heat load is shown in Fig. 8. It can be seen that under various gas turbine output and ambient temperature, for the 1×1 plant, the slope is between 6.73×10^{-2} and 7.13×10^{-2} MW/(GJ/h). The average value is approximately 7.0×10^{-2} MW/(GJ/h) and adopted to calculate the R_{ST}, which equals to 4.970 MW/min. For the 2×1 plant, the slope is between 6.52×10^{-2} and 6.97×10^{-2} MW/(GJ/h), and the average value is approximately 6.7×10^{-2} MW/(GJ/h). The average value is adopted to calculate the R_{ST}, which equals to 13.869 MW/min.

(4) FOZ

The FOZs of two plants when T_A=273.15 K are shown in Fig. 9.

(5) Fuel consumption characteristic

Due to the long calculation time of the plant thermodynamic model, it is not suitable to directly embed the model into the optimization algorithm. Therefore, in this study, firstly the simulation on various operating conditions is performed with the plant thermodynamic model. Then, based on the simulation data, the fuel consumption characteristic is modelled with the least square support vector regression (LSSVR) algorithm. Theoretically, the main boundary parameters of the field operational process of an NGCC plant are plant power load, heat load and ambient temperature. In order to cover various operating conditions of the plant, different values of these three parameters are adopted and cross matched. The ambient temperature varies from 268.15 K to 308.15 K with the interval of 5 K. The corresponding plant power loads under various partload fractions of gas turbine ranging from 0.3 to 1 with the interval of 0.1 are selected. The heat load is divided into 9 equals under each value of ambient temperature and partload fraction of gas turbine. A total of 648 operating conditions of an NGCC plant are simulated.

LSSVR is considered as one of the most robust and accurate methods among the well-known data mining algorithms [63]. It has been increasingly used in research and industry due to its highly effective model in solving non-linear problems with excellent time efficiency [64, 65]. In the modelling process, the K-fold cross validation method is adopted to improve the generalization performance. Details on the LSSVR algorithms used in this study are presented in the work carried out by Cong [66]. The average and maximum relative errors of the fuel consumption LSSVR model for 1×1 plant are 0.05% and 0.25%, respectively. The average and maximum relative errors of the fuel consumption LSSVR model for 2×1 plant are 0.05% and 0.24%, respectively.

4. Results and discussion

4.1 Model validation

4.1.1 Assumptions validation of short-term loads variation process model

As can be seen from Fig. 6, firstly, the delay time of the steam turbine output variation caused by gas turbine is approximately 6 minutes. Based on the statistical results of the field operational data in the recent half year, the maximum time interval between two demands is less than 2.5 minutes. This means in the short-term, the variation of steam turbine output caused by the gas turbine output change has not happened yet. Secondly, the output variation rate of steam turbine caused by gas turbine is approximately 0.6 MW/min. In contrast, the output variation rate of steam turbine caused by heat load change is 4.970 MW/min, much larger than that caused by gas turbine. The output variation rate of gas turbine is 11MW/min. In the power load regulation process, the output variation of steam turbine caused by gas turbine can be rapidly balanced by the gas turbine. Therefore, the rationality of assumptions for the short-term loads variation process model is proved.

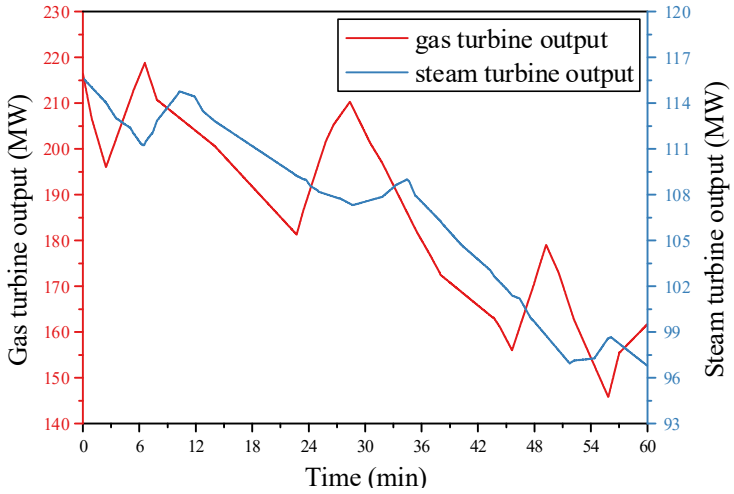

Fig. 6. One-hour field operational data of gas turbine output and steam turbine output of 1×1 plant at condensing mode (non-heat supply).

4.1.2 Validation of short-term loads variation process model

The field and simulated loads variation process of 1×1 plant at four scenarios is shown in Fig. 7. As shown in figures, in comparison with the field operational data, the maximum error of power load variation process is about 2.6 seconds. The maximum error of heat load variation process is less than 1 second. The accuracy and feasibility of the short-term loads variation process model are proved. The reasons for the slightly larger error of power load variation process may be: a) in the calculation of output variation rate of steam turbine, the influence of gas turbine is neglected; b) during the field operation of an NGCC plant, there are fluctuations in some parameters of HRSG, such as water levels of drums, and the time differences between heat exchange processes of different pressure water-steam circuits; c) the coefficient θ_{ST}^{H} is calculated from thermodynamic model, between which and field data there is error; d) it can be seen from the field heat load variation process, there is fluctuation on heat load ramp rate. The above factors will affect the output variation rate of steam turbine, so that the plant power load ramp rate is also influenced.

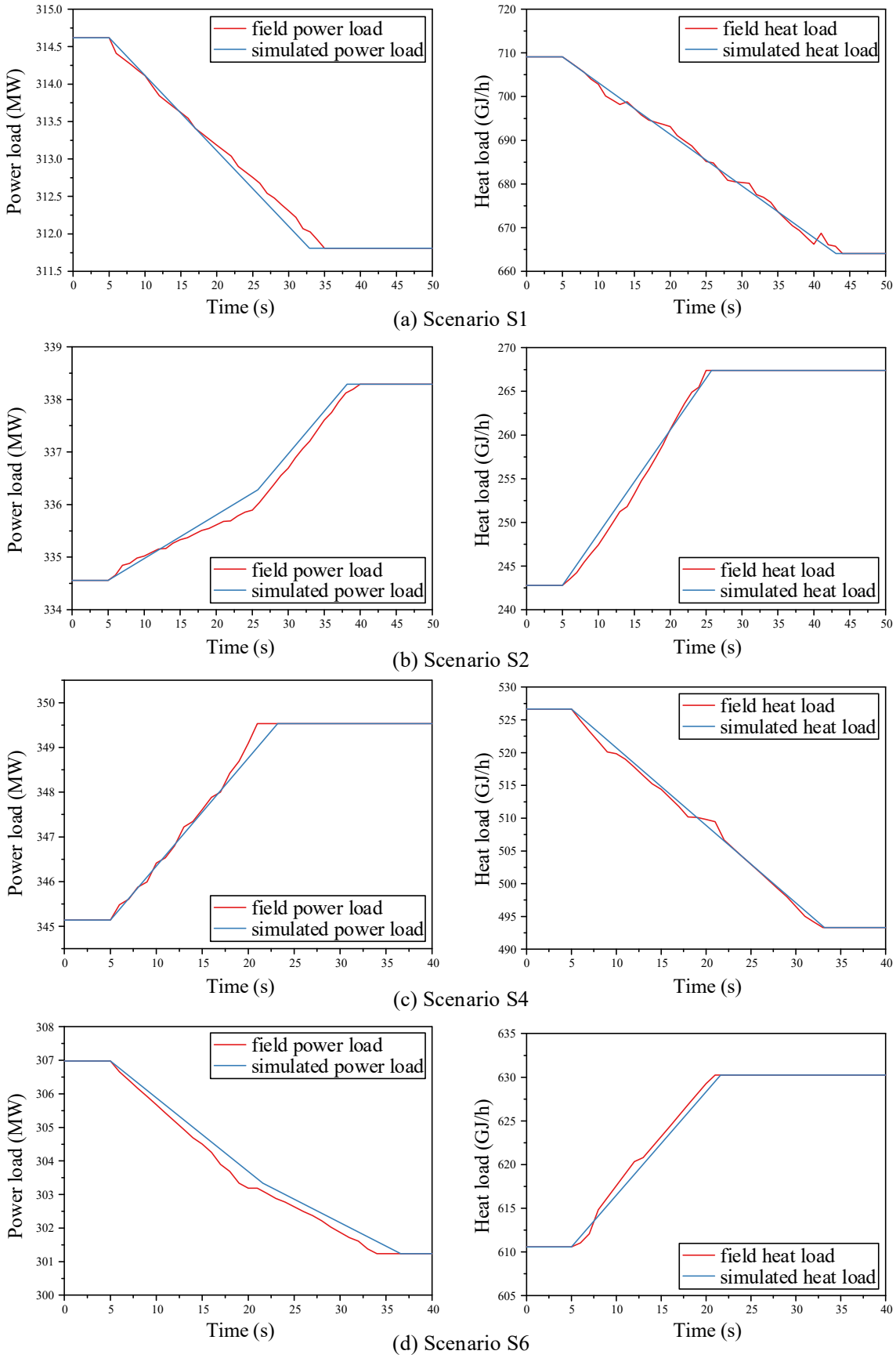

Fig. 7. Field and simulated loads variation process of 1×1 plant at four scenarios.

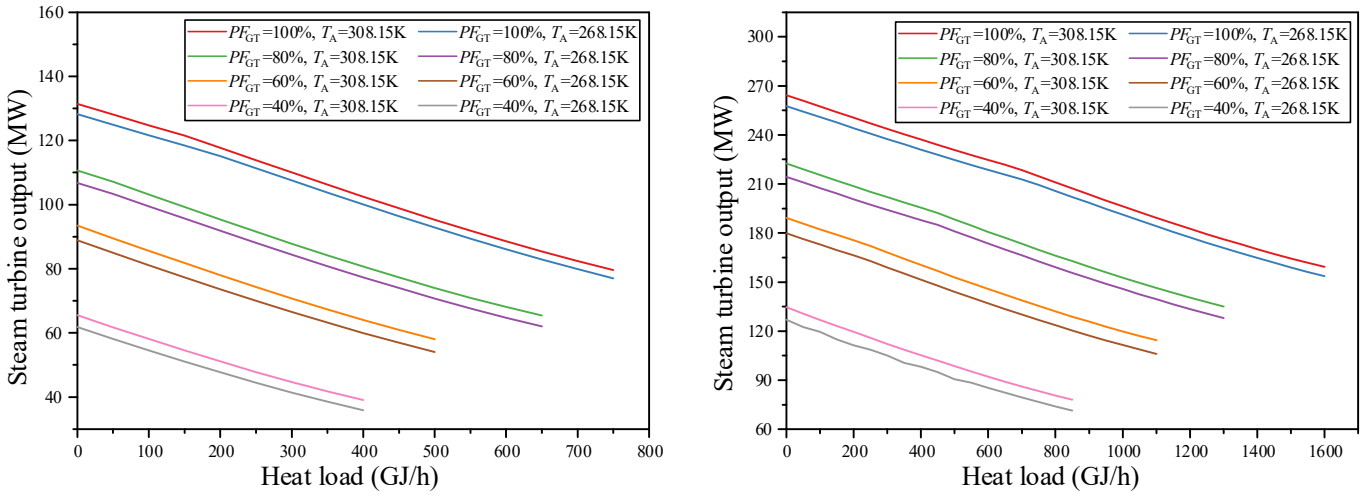

(a) 1×1 plant (b) 2×1 plant

Fig. 8. Relationship between steam turbine output and heat load under various gas turbine output and ambient temperature: (a) 1×1 plant and (b) 2×1 plant.

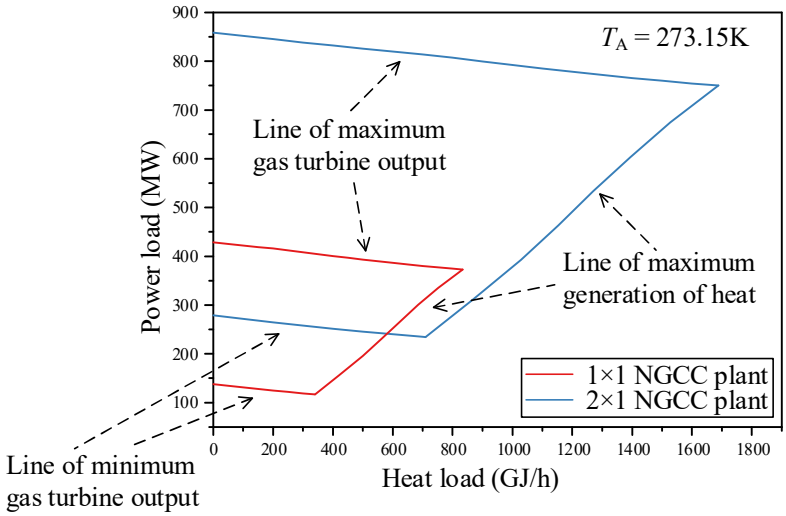

Fig. 9. FOZs of 1×1 and 2×1 NGCC plants.

4.1.3 Validation of plants thermodynamic models

The accuracy and applicability of the plants thermodynamic models are proved by comparing the design data provided by the manufacturer with the simulated values under the same boundary condition. The ambient temperature T_A, gas turbine output P_{GT}, plant heat load Q, and condenser pressure p_{CD} are selected as the boundary condition parameters. The HRSG inlet gas temperature $T_{IN,G}$ and exhaust gas temperature $T_{EX,G}$, HP live steam pressure $p_{LS,HP}$, IP live steam pressure $p_{LS,IP}$, LP live steam pressure $p_{LS,LP}$, steam turbine output P_{ST} and energy utilization efficiency η_{CC} are selected as the validation parameters. It can be seen from the Table S3 and Table S4, most parameter errors are within a tolerable range of 1.5%, with $T_{EX,G}$ of 2×1 plant slightly higher at 1.84%.

4.2 Comparison between the regular and improved CHPED models

CHPED calculation on the one-hour field demands of the power station is performed with the regular and improved model, respectively. Then, on the basis of the CHPED calculation results, the one-hour actual

operation process of two plants is simulated with the short-term loads variation process model. The actual power load variation process and heat load variation process of the power station are shown in Fig. 10 and Fig. 11. For the regular CHPED model, there are 12 power demands and 19 heat demands that fail to be met within the required regulation time limits. There are even 6 power demands and 16 heat demands that fail to be met before next demand arrives. The dispatched demands and actual operation process of two plants under the regular CHPED model are shown in Fig. 12. It can be seen that, due to the enormous difference between the dispatched demand and current load at some times, the plant cannot achieve these demands in time. As a consequence, the demands of the power station cannot be met. The dispatched demands and actual operation process of two plants under the improved CHPED model are shown in Fig. 13. As the practical loads variation capacity of plants has been taken into consideration, all the demands of both plants are achieved in the required regulation time limits. Therefore, the loads variation process of the power station can well meet the requirements of power grid and DH system.

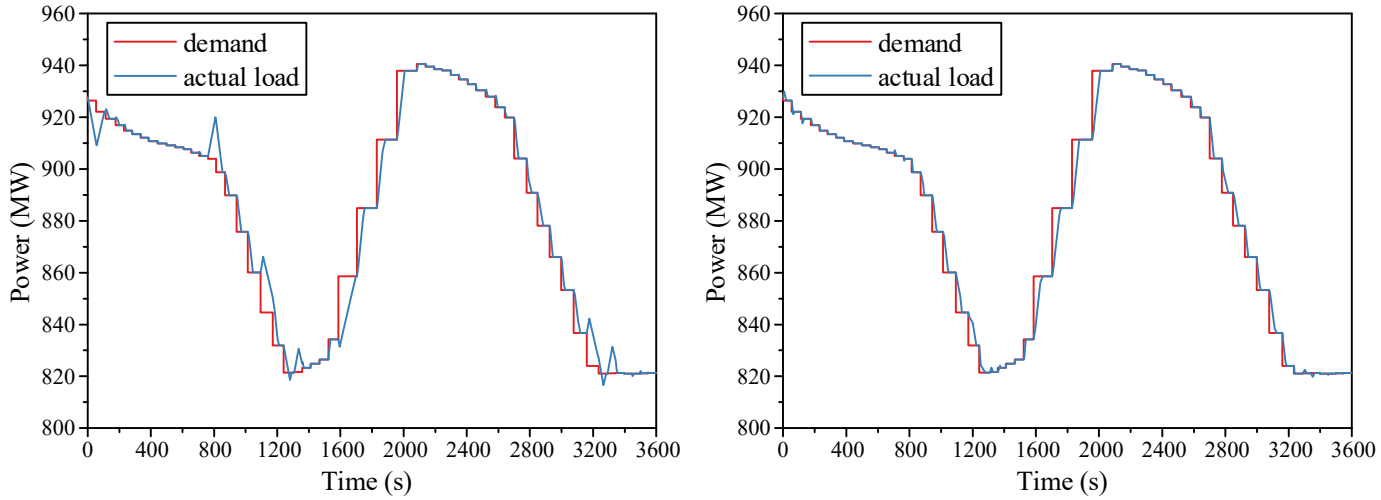

(a) Regular CHPED model (b) Improved CHPED model

Fig. 10. Actual power load variation process of the power station: (a) regular CHPED model and (b) improved CHPED model.

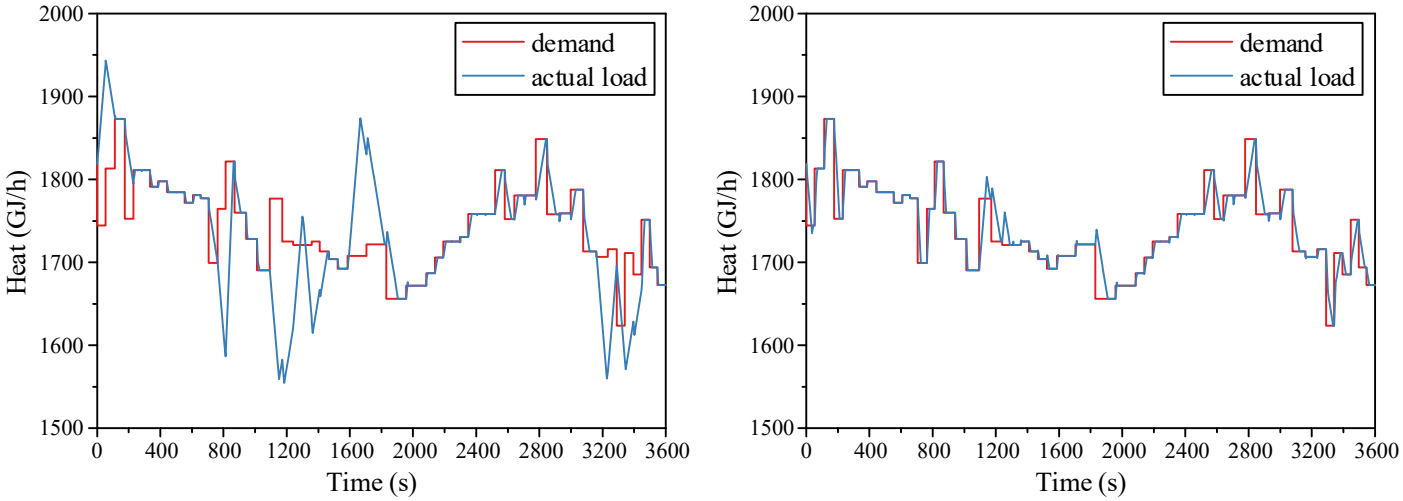

(a) Regular CHPED model (b) Improved CHPED model

Fig. 11. Actual heat load variation process of the power station: (a) regular CHPED model and (b) improved CHPED model.

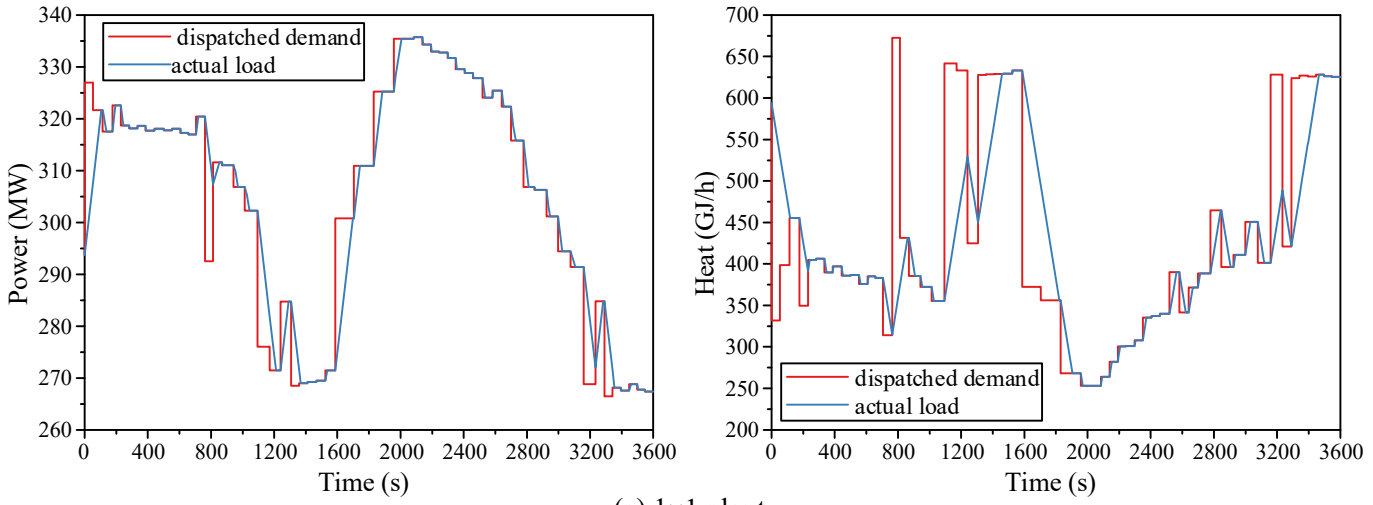

(a) 1×1 plant

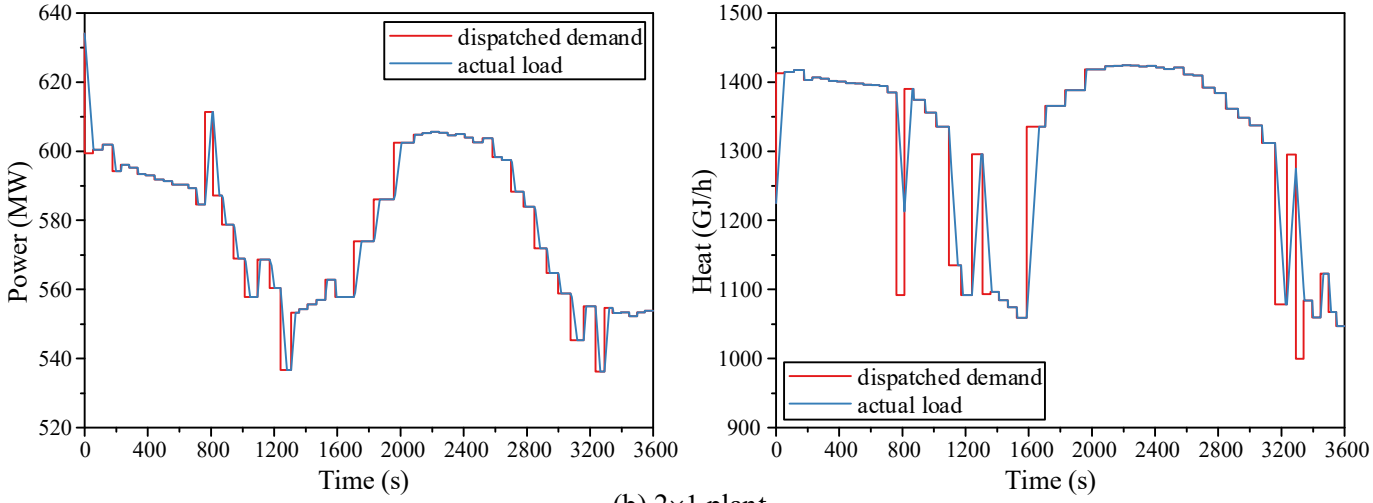

(b) 2×1 plant

Fig. 12. Dispatched demands and actual operation process of (a) 1×1 plant and (b) 2×1 plant under the regular CHPED model.

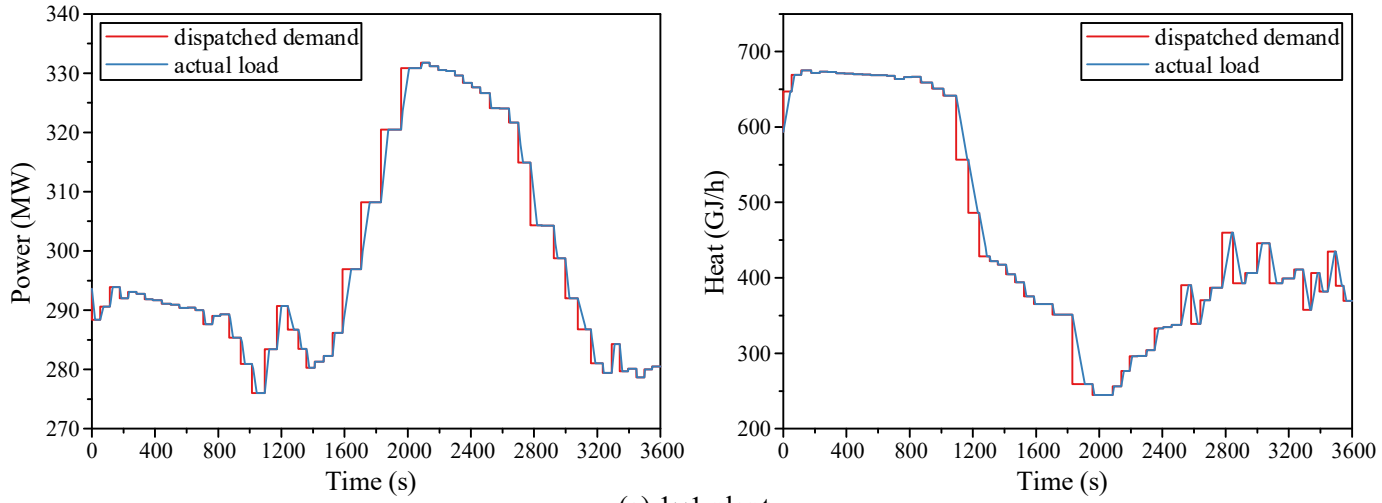

(a) 1×1 plant

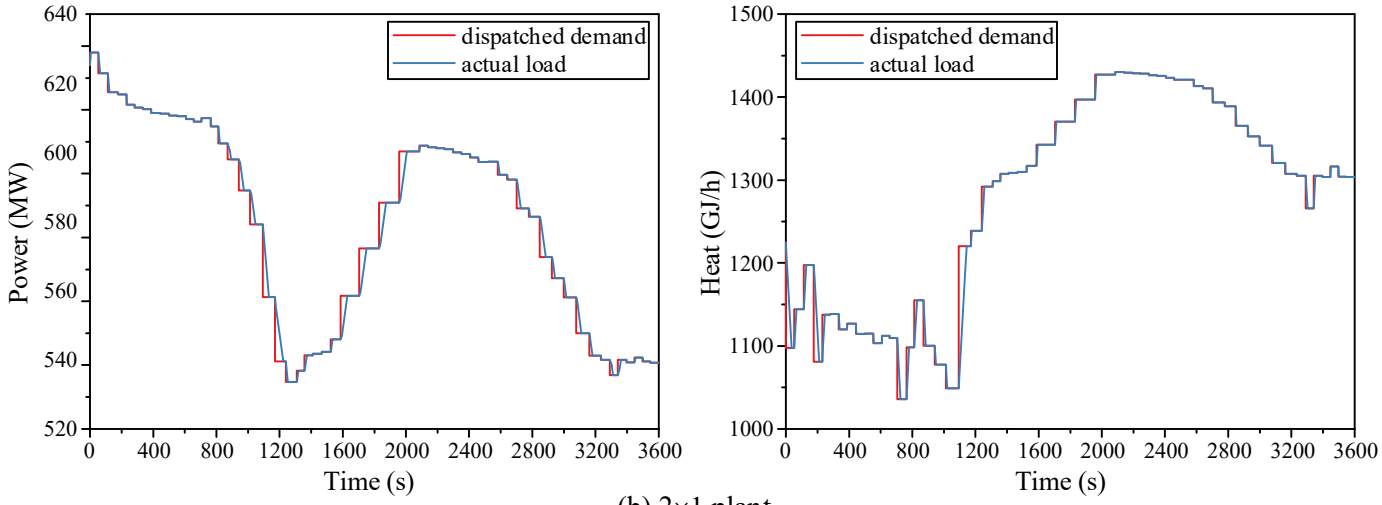

(b) 2×1 plant

Fig. 13. Dispatched demands and actual operation process of (a) 1×1 plant and (b) 2×1 plant under the improved CHPED model.

In order to prove the improvement on economic performance with the improved CHPED model, the fuel consumption of the power station is calculated based on the fuel consumption model of each plant. On the one-hour cumulative fuel consumption, the improved CHPED model can save 171.4 kg (0.12%) over the field operational demands. On the fuel consumption of a single demand, the improved CHPED model can save a maximum of 0.1293 kg/s (0.31%), and a minimum of 0.0038 kg/s (0.01%) over the field operational demands. This shows that the improved CHPED model not only enhances the economic performance, but also ensures the operational reliability and security of the power station.

4.3 Influence of heat load ramp rates on CHPED results

In this section, the influence rules of heat load ramp rates (R_H) on the economic performance of CHPED results is investigated, based on the improved CHPED model. They are further analyzed from the perspective of the principle of the optimization algorithm, so that the reliability of the conclusions is supported. The obtained conclusions can provide theoretical guidance for the field operation of plants on heat load ramp rates adjustment.

According to the short-term loads variation process model, higher R_H will lead to a larger variation range

of heat load in a certain period of time. For the power load, the ramp rate will be influenced greater during heat load variation process. But in the meanwhile, the heat demand will be met earlier, which means the influence time will decrease. As a result, the influence of R_H on the variation range of power load in a certain period of time is the result of a trade-off between influence rate and influence time. Because of the different required regulation time limits from DH system and power grid, the value of "a certain period of time" mentioned above cannot be set. This results in the variation range of heat and power loads of a plant cannot be directly displayed on the FOZ figure. Therefore, the influence of R_H on the economic performance of CHPED results is studied and analyzed through calculation cases. On the basis of the improved CHPED model, the CHPED calculation with different R_H is conducted and compared.

For each demand, the CHPED calculation is performed separately: the field operational loads of plants at the moment when the power station receives the new demand are taken as the initial condition. This ensures that the CHPED calculation for the same demand is set with the same boundary conditions, and the only difference on R_H. The original heat load ramp rates (R_H^O), 71 GJ/h for the 1×1 plant and 207 GJ/h for the 2×1 plant, are taken as the benchmark. The R_H increase from $0.6R_H^O$ to $2R_H^O$ gradually at the interval of $0.2R_H^O$, and the difference in the fuel consumption of the CHPED results before and after R_H increase is calculated (a total of 7 calculation cases). If the difference in fuel consumption is smaller than 0, it means that the increase of R_H leads to a CHPED result with better economic performance. If the difference equals to 0, it means that the CHPED result is unchanged. If the difference is larger than 0, it means that the CHPED result becomes worse. The amount of demands under these three changes in the CHPED result are counted. As can be seen from the Fig. 14, when R_H are low, for most demands the increase of R_H will lead to a CHPED result with better economic performance. There are several demands of which the CHPED result remains unchanged, and no demand of which the CHPED result becomes worse. When R_H are high, after R_H increase, the amount of demands of which the CHPED result becomes better decreases. The amount of demands of which the CHPED result remains unchanged or becomes worse rises. The difference in fuel consumption of each demand in 7 calculation cases is shown in Fig. S3 in supplementary material. The reason for the variation trend showed in Fig. 14 will be analyzed and elaborated below.

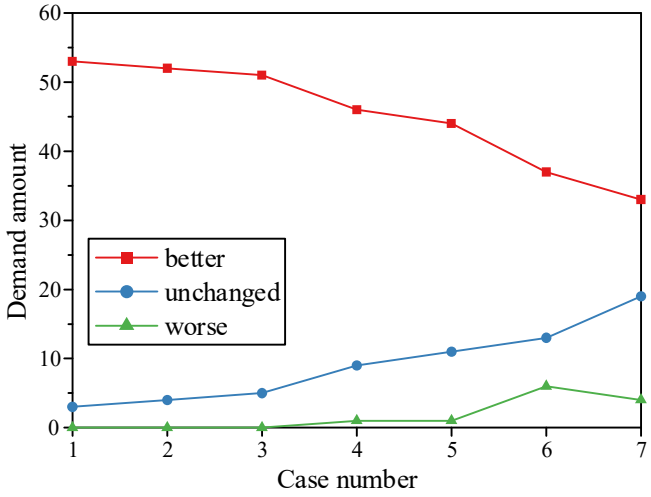

Fig. 14. Amount of demands under three changes in the CHPED result.

In this study, the influence rules and reasons of R_H are investigated from the perspective of the time when the demand is met. Demands are classified into four states, based on the relationship between the time when they are met and the required regulation time limits, as shown in Table 1. Due to the variation of CHPED

results under different R_H, the state of a demand may change. The state of a demand referred in this study is the state corresponding to the CHPED result before the variation of R_H. Statistic calculation on the states of 392 (7×56) demands in all cases is carried out. After the increase of R_H, the changes in economic performance of the CHPED results of the demands at each state are shown in Table 2.

Table 1.

Criteria and characteristics of 4 states of demands.

State	Criteria	Characteristics (the location of the CHPED result)
State1	$\Delta t_{HM}=\Delta t_{DH}$ $\Delta t_{PM}=\Delta t_{PG}$	The location of the CHPED result is on the boundary of the variation range of heat and power loads of the power station.
State2	$\Delta t_{HM}=\Delta t_{DH}$ $\Delta t_{PM}<\Delta t_{PG}$	The location of the CHPED result is on the boundary of the variation range of heat load, and within the variation range of power load of the power station.
State3	$\Delta t_{HM}<\Delta t_{DH}$ $\Delta t_{PM}=\Delta t_{PG}$	The location of the CHPED result is within the variation range of heat load, and on the boundary of the variation range of power load of the power station.
State4	$\Delta t_{HM}<\Delta t_{DH}$ $\Delta t_{PM}<\Delta t_{PG}$	The location of the CHPED result is within the variation range of heat and power loads of the power station.

Δt_{HM} is the time when the heat demand of the power station is met; Δt_{PM} is the time when the power demand of the power station is met; Δt_{DH} is the required regulation time limits from DH system; Δt_{PG} is the required regulation time limits from power grid.

Table 2.

Changes in economic performance of the CHPED results of the demands at each state.

State	Total amount	Changes in economic performance of the CHPED results after the increase of R_H		
		Better	Unchanged	Worse
State1	253	249	0	4
State2	50	50	0	0
State3	43	8	27	8
State4	46	9	37	0

Further, these changes are analyzed from the perspective of the principle of the CST-PSO algorithm. When the optimization result is located on the boundary of the particles' searching range, it is greatly possible that the local optimum is outside the searching range. The optimization result is moving towards the local optimum. Consequently, if the particles' searching range is expanded, the optimization result will be closer to the local optimum. The optimization result will be better. If the particles' searching range is shrunk, the previous optimization result cannot be achieved. The optimization result will be worse. When the optimization result is located within the particles' searching range, it means that the optimization result is one of the local optima. If there is no significant variation on particles' searching range, it is most likely that the optimization result will not change. Therefore, the following conclusions can be drawn: after R_H increase,

(1) For the demands at State1, there is a high probability that the economic performance of their CHPED results will be better, and a low probability that it will be worse. The reason is that their CHPED results are located on the boundary of the variation range of heat and power loads of the power station. As a result, the change in the variation range of heat and power loads can directly affect CHPED results.

The variation range of heat load is proportional to R_H, while the variation range of power load is the result of a trade-off between influence rate and influence time of R_H. The change in the variation range of power load is not as great as that of heat load.

(2) For the demands at State2, the economic performance of their CHPED results will become better. The reason is that their CHPED results are located on the boundary of the variation range of heat load, and within the variation range of power load. As a result, the change in the variation range of heat load can directly affect CHPED results. It is extremely probable that the change in the variation range of power load has no effect on CHPED results.

(3) For the demands at State3, three changes in the economic performance of their CHPED results are all possible. The reason is that their CHPED results are located within the variation range of heat load, and on the boundary of the variation range of power load. As a result, the change in the variation range of power load can directly affect CHPED results. Since the variation range of power load is the combined result of influence rate and influence time of R_H, it may be larger, smaller and unchanged.

(4) For the demands at State4, there is a high probability that the economic performance of their CHPED results will remain unchanged, and a low probability that it will be better. The reason is that their CHPED results are located within the variation range of heat and power load. Only when the change in the variation range of heat and power loads is large enough, can CHPED results be affected.

(5) In conclusion, from the perspective of economic performance of the power station, for the demands at State1 and State2, the increase of R_H is beneficial. For the demands at State3 and State4, it may not be necessary to make adjustment on R_H. Therefore, when R_H are low, the variation range of heat load is small, which leads to most demands at State1 and State2. For these demands, the increase of R_H will lead to a CHPED result with better economic performance. When R_H are high, the variation range of heat load is large, which leads to more demands at State3 and State4. Because of this, the amount of demands of which the CHPED result remains unchanged or becomes worse rises. That is the reason for the variation trend showed in Fig. 14.

With the same method, statistic calculation on the situation after the decrease of R_H is also carried out. As shown in Table S5, the changes in economic performance of the CHPED results are opposite to that in the situation after the increase of R_H, which supports the analysis above.

5. Conclusions

In this work, an improved CHPED model for NGCC plants with consideration on the practical loads variation capacity of plants is developed. In order to ensure the feasibility of dispatched demands, the short-term loads variation process of NGCC plants is modelled based on the power and heat loads control logic in the field operation process. The accuracy of the short-term loads variation process model is proved by comparison with the field operational data, with tolerance intervals of 2.6 seconds for power load and 1 second for heat load. CHPED calculation on one-hour field demands of an NGCC power station is performed with the regular and improved CHPED models, respectively. The comparison and analysis on the CHPED results are conducted. Based on the improved CHPED model, the influence of heat load ramp rates of plants on CHPED results is investigated and analyzed. The main conclusions can be summarized as follows:

(1) The improved CHPED model not only enhances the economic performance, but also ensures the operational reliability and security of plants. With the improved CHPED model, all the 56 field demands in one hour are met in the required regulation time limits. In contrast, with the regular CHPED

model, there are 12 power demands and 19 heat demands that fail to be met within the required regulation time limits. Compared with the field operational demands of plants, the improved CHPED model can save 171.4 kg (0.12%) on one-hour cumulative fuel consumption, and 0.0038-0.1293 kg/s (0.01-0.31%) on the fuel consumption of a single demand. The improved CHPED model can be applied in the real-time field operation of plants to offer guidance as an optimization tool.

(2) The influence rules and reasons of heat load ramp rates on CHPED results are investigated from a time perspective. If the time when the heat demand is met equals to the required regulation time limits from DH system, there is a very high probability that the increase of heat load ramp rates will lead to a CHPED result with better economic performance. Otherwise, it may not be necessary to make adjustment on heat load ramp rates, due to the uncertain variation direction in economic performance of the CHPED result. The influence rules can provide theoretical reference for the field operation of plants on heat load ramp rates adjustment.

Nomenclature

Acronyms	
CHP	combined heat and power
CHPDED	combined heat and power dynamic economic dispatch
CHPED	combined heat and power economic dispatch
CST	chaos searching technique
DH	district heating
FOZ	feasible operating zone
HP	high pressure
HRSG	heat recovery steam generator
IP	intermediate pressure
LP	low pressure
LSSVR	least square support vector regression
NGCC	natural gas combined cycle
PSO	particle swarm optimization
RH	reheat
Symbol	
C	plant fuel cost
P	power load
p	pressure
PF	partload fraction
Q	heat load
R	ramp rate
T	temperature
t	time
α	heat relationship coefficient
β	power relationship coefficient
θ	output variation coefficient
ξ	penalty coefficient
Subscripts	
A	ambient
CD	condenser
D	demand
DE	delay
DH	district heating system
EX	exhaust
G	gas
GT	gas turbine
H	heat load
HM	power station heat demand is met
HP	high pressure
HS	plant heat demand is met
IN	inlet
IP	intermediate pressure
LP	low pressure
LS	live steam
MAX	maximum
MIN	minimum
N	nominal
O	original
P	power load
PG	power grid
PM	power station power demand is met
PS	plant power demand is met
ST	steam turbine

Acknowledgements

This study was supported by the National Natural Science Foundation of China (grant numbers 51976031), the Fundamental from China Scholarship Council (grant numbers 201906090046) and the Qinglan Project of Jiangsu Province, China.

References

[1] Mohammed M K, Awad O I, Rahman M M, et al. The optimum performance of the combined cycle power plant: A comprehensive review[J]. Renewable and Sustainable Energy Reviews, 2017, 79: 459-474.

[2] Gonzalez-Salazar M A, Kirsten T, Prchlik L. Review of the operational flexibility and emissions of gas- and coal-fired power plants in a future with growing renewables[J]. Renewable and Sustainable Energy Reviews, 2018, 82: 1497-1513.

[3] Rúa J, Bui M, Nord L O, et al. Does CCS reduce power generation flexibility? A dynamic study of combined cycles with post-combustion CO2 capture[J]. International Journal of Greenhouse Gas Control, 2020, 95: 102984.

[4] Bao J, Zhang L, Song C, et al. Reduction of efficiency penalty for a natural gas combined cycle power plant with post-combustion CO2 capture: Integration of liquid natural gas cold energy[J]. Energy Conversion and Management, 2019, 198: 111852.

[5] Nazari-Heris M, Mohammadi-Ivatloo B, Asadi S, et al. Large-scale combined heat and power economic dispatch using a novel multi-player harmony search method[J]. Applied Thermal Engineering, 2019, 154: 493-504.

[6] Rúa J, Agromayor R, Hillestad M, et al. Optimal Dynamic Operation of Natural Gas Combined Cycles Accounting for Stresses in Thick-Walled Components[J]. Applied Thermal Engineering, 2020: 114858.

[7] Noussan M, Jarre M, Roberto R, et al. Combined vs separate heat and power production–primary energy comparison in high renewable share contexts[J]. Applied energy, 2018, 213: 1-10.

[8] Hagh M T, Teimourzadeh S, Alipour M, et al. Improved group search optimization method for solving CHPED in large scale power systems[J]. Energy Conversion and Management, 2014, 80: 446-456.

[9] Razavi S E, Javadi M S, Esmaeel Nezhad A. Mixed‐integer nonlinear programming framework for combined heat and power units with nonconvex feasible operating region: Feasibility, optimality, and flexibility evaluation[J]. International Transactions on Electrical Energy Systems, 2019, 29(3): e2767.

[10] Heredia F J, Rider M J, Corchero C. A stochastic programming model for the optimal electricity market bid problem with bilateral contracts for thermal and combined cycle units[J]. Annals of Operations Research, 2012, 193(1): 107-127.

[11] Rist J F, Dias M F, Palman M, et al. Economic dispatch of a single micro-gas turbine under CHP operation[J]. Applied Energy, 2017, 200: 1-18.

[12] Bayón L, García Nieto P J, Grau J M, et al. An economic dispatch algorithm of combined cycle units[J]. International Journal of Computer Mathematics, 2014, 91(2): 269-277.

[13] Lu B, Shahidehpour M. Short-term scheduling of combined cycle units[J]. IEEE Transactions on Power Systems, 2004, 19(3): 1616-1625.

[14] Troy N, Flynn D, OMalley M. Multi-mode operation of combined-cycle gas turbines with increasing wind penetration[J]. IEEE Transactions on power systems, 2011, 27(1): 484-492.

[15] Vithayasrichareon P, MacGill I F. Incorporating short-term operational plant constraints into assessments of future electricity generation portfolios[J]. Applied energy, 2014, 128: 144-155.

[16] Geng Z, Chen Q, Chen X, et al. Environmental economic dispatch towards multiple emissions control coordination considering a variety of clean generation technologies[C]//2015 IEEE Power & Energy Society General Meeting. IEEE, 2015: 1-5.
[17] Pujihatma P, Hadi S P, Rohmat T A. Combined heat and power–multi-objective optimization with an associated petroleum and wet gas utilization constraint[J]. Journal of Natural Gas Science and Engineering, 2018, 54: 25-36.
[18] Lopez J A, Ceciliano-Meza J L, Moya I G, et al. A MIQCP formulation to solve the unit commitment problem for large-scale power systems[J]. International Journal of Electrical Power & Energy Systems, 2012, 36(1): 68-75.
[19] Santos M I, Uturbey W. A practical model for energy dispatch in cogeneration plants[J]. Energy, 2018, 151: 144-159.
[20] Konash O, El-Sharakawi M. Economic dispatch using Particle Swarm Optimization for combined cycle generators[C]//2009 IEEE/PES Power Systems Conference and Exposition. IEEE, 2009: 1-9.
[21] Bragin M A, Luh P B, Yan J H, et al. Novel exploitation of convex hull invariance for solving unit commitment by using surrogate Lagrangian relaxation and branch-and-cut[C]//2015 IEEE Power & Energy Society General Meeting. IEEE, 2015: 1-5.
[22] Bragin M A, Luh P B, Yan J H, et al. Surrogate Lagrangian relaxation and branch-and-cut for unit commitment with combined cycle units[C]//2014 IEEE PES General Meeting| Conference & Exposition. IEEE, 2014: 1-5.
[23] Sukmadi T, Wardhana A D, Riyadi M A. Optimization of gas turbine power plant economic dispatch using Cuckoo Search Algorithm method[C]//2017 4th International Conference on Information Technology, Computer, and Electrical Engineering (ICITACEE). IEEE, 2017: 131-135.
[24] Haghrah A, Nazari-Heris M, Mohammadi-Ivatloo B. Solving combined heat and power economic dispatch problem using real coded genetic algorithm with improved Mühlenbein mutation[J]. Applied Thermal Engineering, 2016, 99: 465-475.
[25] Beigvand S D, Abdi H, La Scala M. Hybrid gravitational search algorithm-particle swarm optimization with time varying acceleration coefficients for large scale CHPED problem[J]. Energy, 2017, 126: 841-853.
[26] Huang Z, Gao Z, Qi L, et al. A Heterogeneous Evolving Cuckoo Search Algorithm for Solving Large-Scale Combined Heat and Power Economic Dispatch Problems[J]. IEEE Access, 2019, 7: 111287-111301.
[27] Zou D, Li S, Kong X, et al. Solving the combined heat and power economic dispatch problems by an improved genetic algorithm and a new constraint handling strategy[J]. Applied energy, 2019, 237: 646-670.
[28] Basu M. Squirrel search algorithm for multi-region combined heat and power economic dispatch incorporating renewable energy sources[J]. Energy, 2019, 182: 296-305.
[29] Wu C, Gu W, Xu Y, et al. Bi-level optimization model for integrated energy system considering the thermal comfort of heat customers[J]. Applied energy, 2018, 232: 607-616.
[30] Zhang R, Jiang T, Li W, et al. Day-ahead scheduling of integrated electricity and district heating system with an aggregated model of buildings for wind power accommodation[J]. IET Renewable Power Generation, 2019, 13(6): 982-989.
[31] Dai Y, Chen L, Min Y, et al. Dispatch model for CHP with pipeline and building thermal energy storage considering heat transfer process[J]. IEEE Transactions on Sustainable Energy, 2018, 10(1): 192-203.

[32] Anand H, Narang N, Dhillon J S. Unit commitment considering dual-mode combined heat and power generating units using integrated optimization technique[J]. Energy Conversion and Management, 2018, 171: 984-1001.
[33] Anand H, Narang N, Dhillon J S. Multi-objective combined heat and power unit commitment using particle swarm optimization[J]. Energy, 2019, 172: 794-807.
[34] Li W, Li T, Wang H, et al. Optimal Dispatch Model Considering Environmental Cost Based on Combined Heat and Power with Thermal Energy Storage and Demand Response[J]. Energies, 2019, 12(5): 817.
[35] Kaur A, Narang N. Optimum generation scheduling of coordinated power system using hybrid optimization technique[J]. Electrical Engineering, 2019, 101(2): 379-408.
[36] Lahdelma R, Hakonen H. An efficient linear programming algorithm for combined heat and power production[J]. European Journal of Operational Research, 2003, 148(1): 141-151.
[37] Bischi A, Taccari L, Martelli E, et al. A detailed MILP optimization model for combined cooling, heat and power system operation planning[J]. Energy, 2014, 74: 12-26.
[38] Elsido C, Bischi A, Silva P, et al. Two-stage MINLP algorithm for the optimal synthesis and design of networks of CHP units[J]. Energy, 2017, 121: 403-426.
[39] Jena C, Basu M, Panigrahi C K. Differential evolution with Gaussian mutation for combined heat and power economic dispatch[J]. Soft Computing, 2016, 20(2): 681-688.
[40] Yu J, Shen X, Sun H. Economic dispatch for regional integrated energy system with district heating network under stochastic demand[J]. IEEE Access, 2019, 7: 46659-46667.
[41] Sun Y, Xu C, Xu G, et al. A comprehensive thermodynamic analysis of load‐flexible CHP plants using district heating network[J]. International Journal of Energy Research, 2019, 43(9): 4613-4629.
[42] Murugan R, Mohan M R, Rajan C C A, et al. Hybridizing bat algorithm with artificial bee colony for combined heat and power economic dispatch[J]. Applied Soft Computing, 2018, 72: 189-217.
[43] Chen Y, Guo Q, Sun H, et al. A water mass method and its application to integrated heat and electricity dispatch considering thermal inertias[J]. Energy, 2019, 181: 840-852.
[44] Arrieta F R P, Lora E E S. Influence of ambient temperature on combined-cycle power-plant performance[J]. Applied energy, 2005, 80(3): 261-272.
[45] Popli S, Rodgers P, Eveloy V. Trigeneration scheme for energy efficiency enhancement in a natural gas processing plant through turbine exhaust gas waste heat utilization[J]. Applied Energy, 2012, 93: 624-636.
[46] Alobaid F, Starkloff R, Pfeiffer S, et al. A comparative study of different dynamic process simulation codes for combined cycle power plants–Part A: Part loads and off-design operation[J]. Fuel, 2015, 153: 692-706.
[47] Shin J Y, Jeon Y J, Maeng D J, et al. Analysis of the dynamic characteristics of a combined-cycle power plant[J]. Energy, 2002, 27(12): 1085-1098.
[48] Montañés R M, GarÐarsdóttir S Ó, Normann F, et al. Demonstrating load-change transient performance of a commercial-scale natural gas combined cycle power plant with post-combustion CO2 capture[J]. International Journal of Greenhouse Gas Control, 2017, 63: 158-174.
[49] Wan Z, Wang G, Sun B. A hybrid intelligent algorithm by combining particle swarm optimization with chaos searching technique for solving nonlinear bilevel programming problems[J]. Swarm and Evolutionary Computation, 2013, 8: 26-32.
[50] Alatas B, Akin E, Ozer A B. Chaos embedded particle swarm optimization algorithms[J]. Chaos, Solitons & Fractals, 2009, 40(4): 1715-1734.

[51] Gandomi A H, Yun G J, Yang X S, et al. Chaos-enhanced accelerated particle swarm optimization[J]. Communications in Nonlinear Science and Numerical Simulation, 2013, 18(2): 327-340.
[52] Cai J, Ma X, Li L, et al. Chaotic particle swarm optimization for economic dispatch considering the generator constraints[J]. Energy conversion and management, 2007, 48(2): 645-653.
[53] Si F, Gu H, Ye Y, et al. Online unit load economic dispatch based on chaotic-particle swarm optimization algorithm[C]//Zhongguo Dianji Gongcheng Xuebao(Proceedings of the Chinese Society of Electrical Engineering). Chinese Society for Electrical Engineering, 2011, 31(26): 103-109.
[54] Ebsilon Professional. https://www.ebsilon.com/en [accessed February 11, 2020].
[55] Xue Y, Ge Z, Yang L, et al. Peak shaving performance of coal-fired power generating unit integrated with multi-effect distillation seawater desalination[J]. Applied Energy, 2019, 250: 175-184.
[56] Zhao S, Ge Z, He J, et al. A novel mechanism for exhaust steam waste heat recovery in combined heat and power unit[J]. Applied Energy, 2017, 204: 596-606.
[57] Chen X, Chen Q, Chen H, et al. Heat current method for analysis and optimization of heat recovery-based power generation systems[J]. Energy, 2019, 189: 116209.
[58] Hu H, Li Z, Jiang Y, et al. Thermodynamic characteristics of thermal power plant with hybrid (dry/wet) cooling system[J]. Energy, 2018, 147: 729-741.
[59] Tashtoush B, Algharbawi A B R. Parametric Study of a Novel Hybrid Solar Variable Geometry Ejector Cooling with Organic Rankine Cycles[J]. Energy Conversion and Management, 2019, 198: 111910.
[60] Zhai R, Li C, Qi J, et al. Thermodynamic analysis of CO2 capture by calcium looping process driven by coal and concentrated solar power[J]. Energy Conversion and Management, 2016, 117: 251-263.
[61] Yu H, Zhou J, Ma H, et al. Performance analysis and optimization of a NGCC-CHP plant with low pressure economizer partial recirculation system[J]. Energy conversion and management, 2019, 180: 524-532.
[62] Wang J, You S, Zong Y, et al. Flexibility of combined heat and power plants: A review of technologies and operation strategies[J]. Applied energy, 2019, 252: 113445.
[63] The top ten algorithms in data mining[M]. CRC press, 2009.
[64] Zhao H, Magoulès F. A review on the prediction of building energy consumption[J]. Renewable and Sustainable Energy Reviews, 2012, 16(6): 3586-3592.
[65] Ahmad A S, Hassan M Y, Abdullah M P, et al. A review on applications of ANN and SVM for building electrical energy consumption forecasting[J]. Renewable and Sustainable Energy Reviews, 2014, 33: 102-109.
[66] Yu C. Research on Combustion Optimization and Low NOx Emission Control for Utility Boilers[D]. Southeast University (Nanjing, China). 2019

Supplementary material information to

An improved combined heat and power economic dispatch model for natural gas combined cycle power plants

Haiquan Yu[1, 2], Lars O. Nord [2], Cong Yu[3], Jianxin Zhou [1], Fengqi Si[1, *]

[1] Key Laboratory of Energy Thermal Conversion and Control of Ministry of Education, School of Energy and Environment, Southeast University, Nanjing, 210096, P.R. China

[2] Department of Energy and Process Engineering, Norwegian University of Science and Technology - NTNU, Trondheim, Norway

[3] Key Laboratory of industrial soot pollution control in Hubei Province, School of Chemistry and Environmental Engineering, Jianghan University, Wuhan, 430056, P.R. China

Corresponding author at:

E-mail addresses: fqsi@seu.edu.cn (Prof. Dr. Fengqi Si), yhq@seu.edu.cn (Haiquan Yu)

Address: School of Energy & Environment, Southeast University, No.2 Sipailou Road, Nanjing, 210096, China.

Tel: +86 25 83790579.

S1. Implementation of CST-PSO algorithm on CHPED problem

S1.1 CST-PSO algorithm

The particle swarm optimization algorithm with chaos searching technique (CST-PSO) algorithm is developed from the particle swarm optimization (PSO) algorithm. PSO algorithm is easy to trap into the local optima. In order to overcome this defect, researchers embedded chaos searching technique (CST) into PSO [49-53]. The CST has many advantages such as strong randomness, fast convergence and insensitivity to initial parameters. The particle position update process is improved with the help of CST, so that higher accuracy and convergence rate of the solution are achieved. The implementation of CST-PSO algorithm on ED problems has been well validated with outstanding effectiveness and robustness in [52, 53]. The mathematical formulations of CST-PSO algorithm used in this study are shown as follows.

Suppose that the amount of particles in a D-dimensional search space is N. The position of the nth particle can be represented by a D-dimensional vector, $\boldsymbol{X}_n = (x_{n,1}, x_{n,2}, \ldots, x_{n,D})$. The velocity of this particle can be represented by another D-dimensional vector, $\boldsymbol{V}_n = (v_{n,1}, v_{n,2}, \ldots, v_{n,D})$. The best previously visited position of the nth particle is denoted as $\boldsymbol{pbest}_n$. The best previously visited position of all particles is denoted as $\boldsymbol{gbest}$. For the nth particle, the velocity and position at (k+1)th iteration are calculated based on the following equations:

$$\boldsymbol{V}_n(k+1) = \omega(k)\boldsymbol{V}_n(k) + c_1 r_1(k)\left(\boldsymbol{pbest}_n(k) - \boldsymbol{X}_n(k)\right) + c_2 r_2(k)\left(\boldsymbol{gbest}(k) - \boldsymbol{X}_n(k)\right) \tag{1}$$

$$\boldsymbol{X}_n(k+1) = \boldsymbol{X}_n(k) + \boldsymbol{V}_n(k+1) \tag{2}$$

where c_1 and c_2 are positive constants, called acceleration coefficients. r_1 and r_2 are two independent random numbers, uniformly distributed in [0,1]. ω is the inertia weight that controls the impact of previous velocity on current one. In order to achieve a trade-off between exploration and exploitation, the adaptive inertia weight factor is adopted, and can be calculated as:

$$\omega = \begin{cases} \omega_{\mathrm{MIN}} + \dfrac{(\omega_{\mathrm{MAX}} - \omega_{\mathrm{MIN}})(f - f_{\mathrm{MIN}})}{f_{\mathrm{AVG}} - f_{\mathrm{MIN}}} & f \le f_{\mathrm{AVG}} \\ \omega_{\mathrm{MAX}} & f > f_{\mathrm{AVG}} \end{cases} \tag{3}$$

where ω_{MAX} and ω_{MIN} denote the maximum and minimum of ω respectively. f is the current fitness value of the particle. f_{AVG} and f_{MIN} are the average and minimum fitness value of all particles, respectively.

The Logistic map is adopted to generate the D-dimensional chaos vector, $\boldsymbol{Z} = (z_1, z_2, \ldots, z_D)$, shown as the following equation:

$$\boldsymbol{Z}(m+1) = \mu \boldsymbol{Z}(m).\times\left(1 - \boldsymbol{Z}(m)\right) \tag{4}$$

where m is the times of iteration. μ is the control parameter. It has been testified that the system is entirely in chaos situation when $\mu = 4$ and $z \notin \{0, 0.25, 0.5, 0.75, 1\}$.

The chaos vector $\boldsymbol{Z}$ is utilized in the following two processes of PSO algorithm:

(a) The particle position is initialized using $\boldsymbol{Z}$:

$$\boldsymbol{X}_n(1) = \boldsymbol{X}_{\mathrm{MIN}} + \left(\boldsymbol{X}_{\mathrm{MAX}} - \boldsymbol{X}_{\mathrm{MIN}}\right).\times \boldsymbol{Z} \tag{5}$$

(b) After the fitness function calculation and the update of $\boldsymbol{pbest}_n$ of nth particle at kth iteration, iterative

chaos searching is performed around the $\boldsymbol{pbest}_n$:

$$\boldsymbol{X}_n(k,m) = \boldsymbol{pbest}_n(k) + \gamma\left(\boldsymbol{Z}(m) - 0.5\right). \times \boldsymbol{pbest}_n(k) \tag{6}$$

where γ is neighbor radius. If the fitness value of $\boldsymbol{X}_n(k,m)$ is better than that of $\boldsymbol{pbest}_n(k)$, the $\boldsymbol{pbest}_n(k)$ will be updated to $\boldsymbol{X}_n(k,m)$.

S1.2 Particle position correction strategy

In the implementation of CST-PSO algorithm on CHPED models, the optimization variables manipulated by the algorithm are the heat and power demands of each NGCC plant. Suppose that there are (B+C) NGCC plants in the CHPED calculation, B of which are operated at backpressure mode and C are operated at extraction-condensing mode. The number of the plants at backpressure mode is b (b=1, 2, …, B), and the number of the plants at extraction-condensing mode is c (c=1, 2, …, C). The power load and heat load of the plant at backpressure mode are one-to-one correspondence. Consequently, the independent variables of CHPED problem are power demands of all plants ($P_{\mathrm{D},i}(t_0)$) and heat demands of plants at extraction-condensing mode ($Q_{\mathrm{D},c}(t_0)$). The heat demands of plants at backpressure mode ($Q_{\mathrm{D},b}(t_0)$) can be calculated based on their power demands ($P_{\mathrm{D},b}(t_0)$). In the constraints handling process, firstly a particle position correction strategy is proposed to improve the calculation efficiency. The corrected position will fully satisfy the constraints (1), (2) and (3). Then the violation of constraint (4) is checked, if so, the fitness value of this particle will be set to be a penalty coefficient. The penalty coefficient is commonly set to be a very large constant, such as 10^{10}.

In the CST-PSO algorithm, random numbers are included in the calculation processes of particle initialization, velocity update and chaos search around ***pbest***. As a result, the particle position is difficult to satisfy the constraints (1) and (2) (equality constraints), and even violates the constraint (3) (inequality constraint). In order to improve the CHPED model calculation efficiency, for the particle that violates the constraints (1), (2) and (3), a particle position correction strategy is proposed in this study. The strategy works by the following steps:

Step1: Preliminary correction of $P_{\mathrm{D},i}(t_0)$

$$\Delta P_{\mathrm{D,PG}}(t_0) = P_{\mathrm{D,PG}}(t_0) - \sum_{i=1,2,\cdots}^{B+C} P_{\mathrm{D},i}(t_0)$$

$$P_{\mathrm{D},i}(t_0) = P_{\mathrm{D},i}(t_0) + \frac{\Delta P_{\mathrm{D,PG}}(t_0)}{B+C}, \quad \forall i \in [1,2,\cdots,B+C]$$

Step2: Violation of plant capacity limits for $P_{\mathrm{D},i}(t_0)$ is checked

$L_1 = 0$
$L_2 = 0$
for $i = 1:1:B+C$
  if $\left(P_{\mathrm{D},i}\left(t_0\right) > P_{\mathrm{MAX},i}\right)$
    $L_1 = L_1 + 1$
    if $\left(\Delta P_{\mathrm{D,PG}}\left(t_0\right) \geq 0\right)$
      $P_{\mathrm{D},i}\left(t_0\right) = P_{\mathrm{MAX},i}$
      $L_2 = L_2 + 1$
    end if
  end if
  if $\left(P_{\mathrm{D},i}\left(t_0\right) < P_{\mathrm{MIN},i}\right)$
    $L_1 = L_1 + 1$
    if $\left(\Delta P_{\mathrm{D,PG}}\left(t_0\right) \leq 0\right)$
      $P_{\mathrm{D},i}\left(t_0\right) = P_{\mathrm{MIN},i}$
      $L_2 = L_2 + 1$
    end if
  end if
end for

where $P_{\mathrm{MAX},i}$ and $P_{\mathrm{MIN},i}$ are the maximum and minimum power generation capacity on the FOZ. L_1 is the amount of power demands that violate the capacity limits. L_2 is the amount of power demands that are corrected in this step.

Step3: Secondary correction. For the power demands that are not corrected in Step2, corrections are made in this step.

$$\Delta P_{\mathrm{D,PG}}\left(t_0\right) = P_{\mathrm{D,PG}}\left(t_0\right) - \sum_{i=1,2,\cdots}^{B+C} P_{\mathrm{D},i}\left(t_0\right)$$

$$P_{\mathrm{D},i}\left(t_0\right) = P_{\mathrm{D},i}\left(t_0\right) + \frac{\Delta P_{\mathrm{D,PG}}\left(t_0\right)}{B+C-L_2}, \quad \forall i \in \left[1,2,\cdots,B+C-L_2\right]$$

Step4: If ($L_1 > 0$), return to Step2, otherwise go to Step5.

Step5: The heat demands of plants at backpressure mode ($Q_{\mathrm{D},b}(t_0)$) are calculated based on their power demands ($P_{\mathrm{D},b}(t_0)$). The maximum and minimum heat generation capacity of each plant at extraction-condensing mode ($Q_{\mathrm{MAX},c}$ and $Q_{\mathrm{MIN},c}$) are calculated based on its power demand ($P_{\mathrm{D},c}(t_0)$).

Step6: Check the rationality of $P_{\mathrm{D},i}(t_0)$ based on $Q_{\mathrm{D},b}(t_0)$, $Q_{\mathrm{MAX},c}$ and $Q_{\mathrm{MIN},c}$. If the portfolio of $P_{\mathrm{D},i}(t_0)$ is not rational, the fitness value of this particle is set to be the penalty coefficient (ξ) directly, and end the correction calculation.

$$\text{if}\left(Q_{\mathrm{D,DH}}(t_0)-\sum_{b=1,2,\cdots}^{B}Q_{\mathrm{D},b}(t_0)>\sum_{c=1,2,\cdots}^{C}Q_{\mathrm{MAX},c}\right)\|\left(Q_{\mathrm{D,DH}}(t_0)-\sum_{b=1,2,\cdots}^{B}Q_{\mathrm{D},b}(t_0)<\sum_{c=1,2,\cdots}^{C}Q_{\mathrm{MIN},c}\right)$$

$fitness=\xi$

end if

Step7: Preliminary correction of $Q_{\mathrm{D},c}(t_0)$

$$\Delta Q_{\mathrm{D,DH}}(t_0)=Q_{\mathrm{D,DH}}(t_0)-\sum_{b=1,2,\cdots}^{B}Q_{\mathrm{D},b}(t_0)-\sum_{c=1,2,\cdots}^{C}Q_{\mathrm{D},c}(t_0)$$

$$Q_{\mathrm{D},c}(t_0)=Q_{\mathrm{D},c}(t_0)+\frac{\Delta Q_{\mathrm{D,DH}}(t_0)}{C},\quad \forall c\in[1,2,\cdots,C]$$

Step8: Violation of plant capacity limits for $Q_{\mathrm{D},c}(t_0)$ is checked

$L_1=0$
$L_2=0$
for $c=1:1:C$
  if $\left(Q_{\mathrm{D},c}(t_0)>Q_{\mathrm{MAX},c}\right)$
    $L_1=L_1+1$
    if $\left(\Delta Q_{\mathrm{D,DH}}(t_0)\geq 0\right)$
      $Q_{\mathrm{D},c}(t_0)=Q_{\mathrm{MAX},c}$
      $L_2=L_2+1$
    end if
  end if
  if $\left(Q_{\mathrm{D},c}(t_0)<Q_{\mathrm{MIN},c}\right)$
    $L_1=L_1+1$
    if $\left(\Delta Q_{\mathrm{D,DH}}(t_0)\leq 0\right)$
      $Q_{\mathrm{D},c}(t_0)=Q_{\mathrm{MIN},c}$
      $L_2=L_2+1$
    end if
  end if
end for

Step9: Secondary correction. For the heat demands that are not corrected in Step8, corrections are made in this step.

$$\Delta Q_{\mathrm{D,DH}}(t_0)=Q_{\mathrm{D,DH}}(t_0)-\sum_{b=1,2,\cdots}^{B}Q_{\mathrm{D},b}(t_0)-\sum_{c=1,2,\cdots}^{C}Q_{\mathrm{D},c}(t_0)$$

$$Q_{\mathrm{D},c}(t_0)=Q_{\mathrm{D},c}(t_0)+\frac{\Delta Q_{\mathrm{D,DH}}(t_0)}{C-L_2},\quad \forall c\in[1,2,\cdots,C-L_2]$$

Step10: If ($L_1>0$), return to Step8, otherwise end the correction calculation. The corrected position will

fully satisfy the constraints (1), (2) and (3).

S1.3 Steps of the improved CHPED model with CST-PSO algorithm

The calculation steps of the improved CHPED model using the above CST-PSO algorithm and particle position correction strategy are as follows, and the flowchart is shown in Fig. S1:

Step1: All particle positions are randomly initialized with the help of CST.

Step2: All particle positions are corrected.

Step3: For each particle, violation of constraint (4) is checked using the short-term loads variation process model.

Step4: Fitness function of each particle is calculated. f_{AVG}, f_{MIN}, $\boldsymbol{pbest}_n$ and $\boldsymbol{gbest}$ are assigned initially.

Step5: For the nth particle, ω and $\boldsymbol{V}_n$ are calculated, and $\boldsymbol{X}_n$ is updated.

Step6: Position of the nth particle is corrected.

Step7: For the nth particle, violation of constraint (4) is checked using the short-term loads variation process model.

Step8: Fitness function of the nth particle is calculated and $\boldsymbol{pbest}_n$ is updated.

Step9: For the $\boldsymbol{pbest}_n$, local search is conducted using CST. The searched position is also corrected and checked for constraint (4) before its fitness function calculation. After that $\boldsymbol{pbest}_n$ is updated.

Step10: After all particles are traversed, f_{AVG}, f_{MIN} and $\boldsymbol{gbest}$ are updated.

Step11: Return to Step5 and start the next iteration of calculation, until the number of iterations meets the requirement.

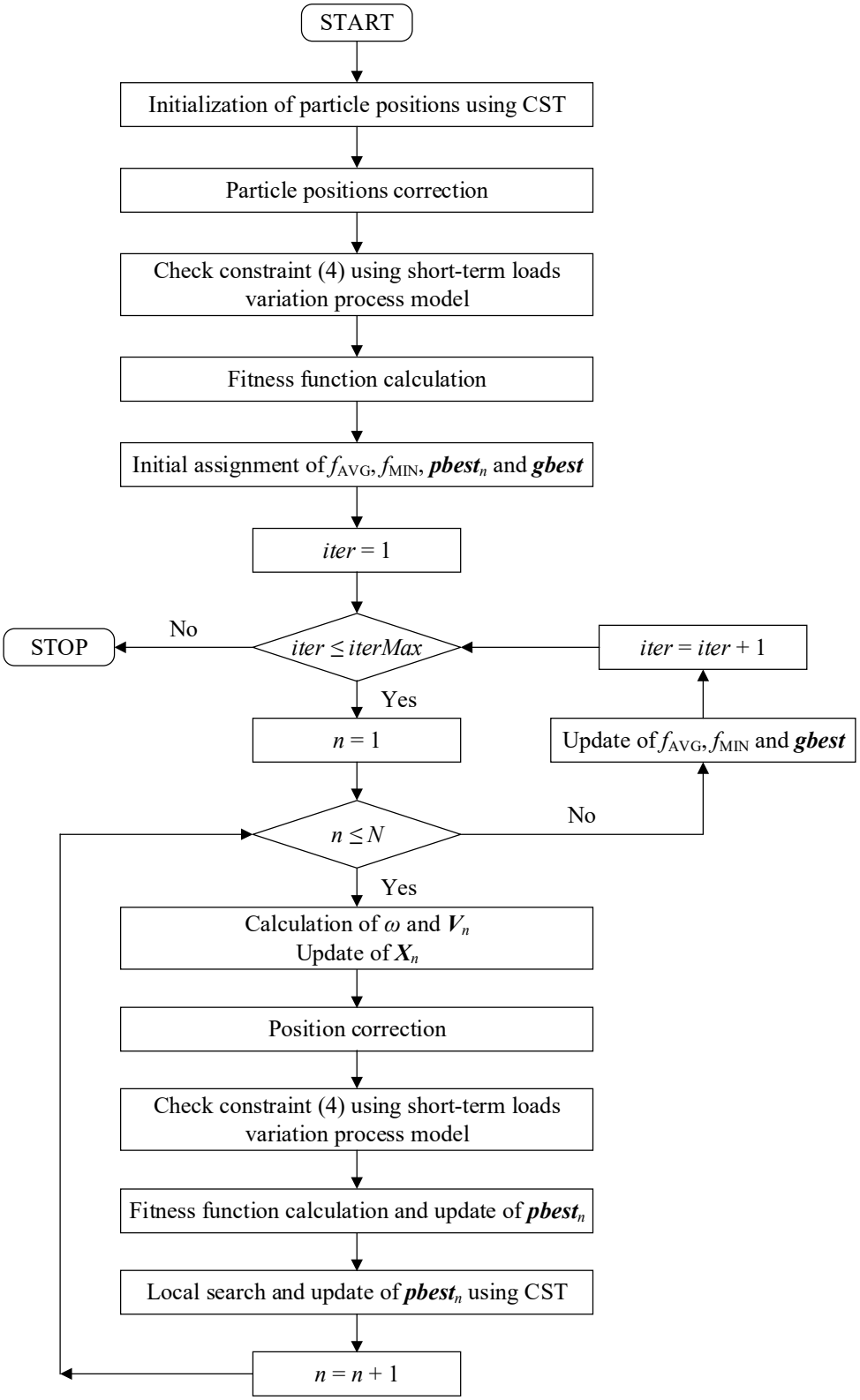

Fig. S1. Flowchart of the improved CHPED model with CST-PSO algorithm.

S2. Technical parameters of 1×1 and 2×1 NGCC plants

Table S1

Technical parameters of 1×1 and 2×1 NGCC plants at design condition.

Items	Parameters	Unit	Values	
			1×1plant	2×1plant
Compressor inlet	temperature	K	288.15	288.15
Gas turbine	power	MW	288.44	288.44
	Efficiency	%	39.38	39.38
	speed	rpm	3000	3000
Gas Turbine exhaust gas	temperature	K	853.55	853.55
	flow	kg/s	692.38	692.38
HP steam	temperature	K	825.65	825.65
	pressure	MPa	12.912	13.362
	flow	kg/s	72.75	73.51
IP steam	temperature	K	598.15	600.55
	pressure	MPa	3.236	3.412
	flow	kg/s	16.78	16.01
LP steam	temperature	K	515.05	515.05
	pressure	MPa	0.528	0.697
	flow	kg/s	12.36	11.96
RH steam	temperature	K	822.95	823.15
	pressure	MPa	3.127	3.262
	flow	kg/s	89.53	89.51
Pinch point	HP	K	11	9
	IP	K	11	9
	LP	K	13	11
Approach temperature difference	HP	K	15	12
	IP	K	15	12
	LP	K	16	13
Steam turbine	power	MW	136.95	275.43
HP cylinder	isentropic efficiency	%	84.0	87.2
IP cylinder	isentropic efficiency	%	92.5	94.8
LP cylinder	isentropic efficiency	%	89.0	87.9

Table S2

The composition and LHV of fuel

CH_4 (%)	C_2H_6 (%)	C_3H_8 (%)	CO_2 (%)	H_2O (%)	LHV (kJ/kg)
95.949	0.908	0.137	3.000	0.006	46087.7

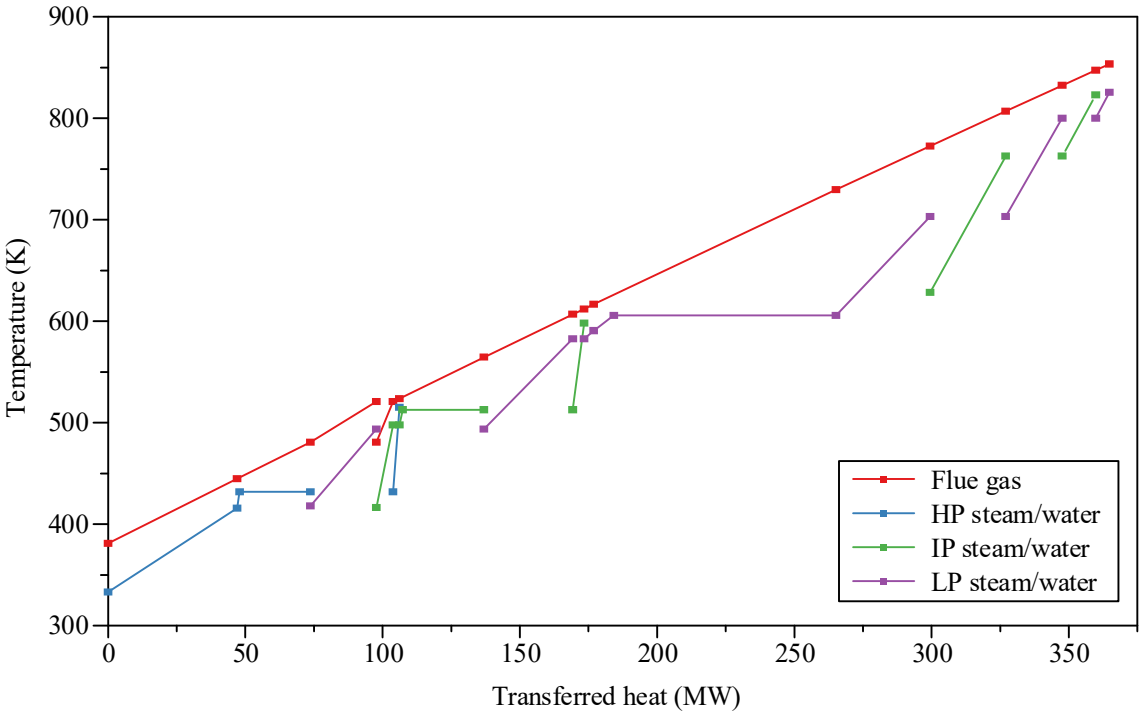

(a) 1×1 plant

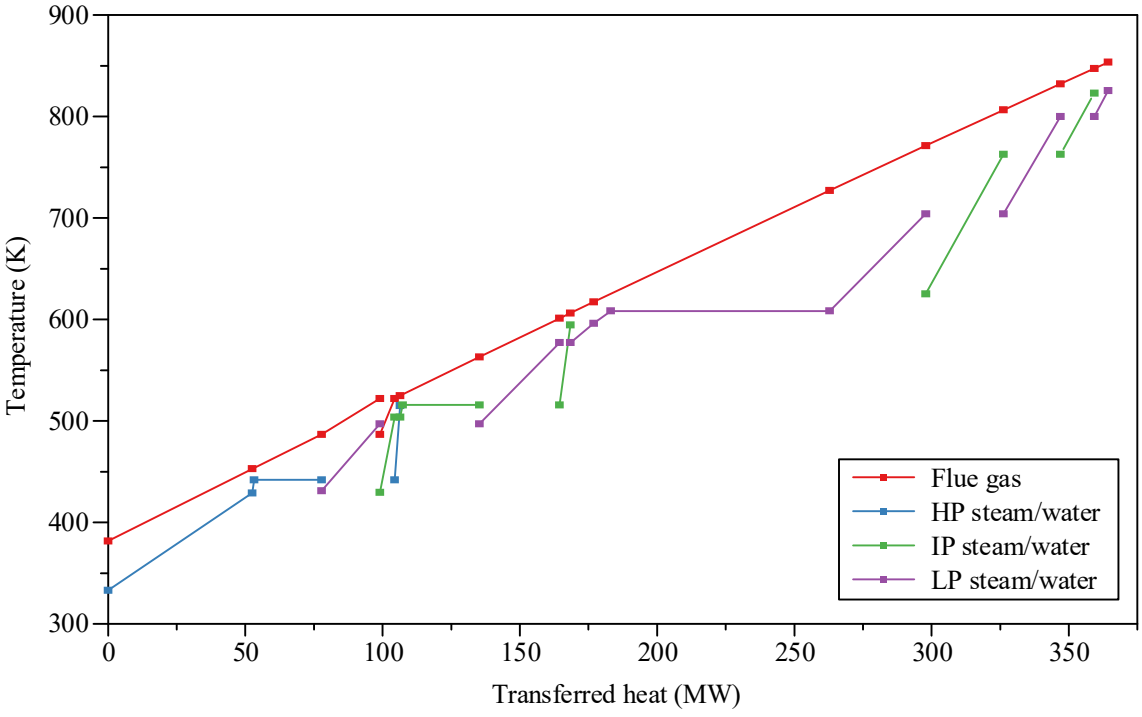

(b) 2×1 plant

Fig. S2. T-Q diagrams of the HRSGs in two NGCC plants at design condition (T_A=288.15 K, 100% gas turbine load without heat load).

S3. Validation of thermodynamic models of NGCC plants

Table S3

Comparison between simulation results and design data (provided by the manufacturer) of 1×1 plant at various conditions.

Item			Unit	PF_{GT} = 100%	PF_{GT} = 75%	PF_{GT} = 50%	PF_{GT} = 30%
Boundary conditions	T_A		K	269.0	269.0	269.0	269.0
	P_{GT}		MW	297.67	223.22	148.80	89.28
	Q		GJ/h	820.44	643.32	493.85	328.71
	p_{CD}		kPa	3.6	3.6	3.6	3.6
Validation parameters	$T_{IN,G}$	Design value	K	817.5	817.5	801.3	700.1
		Simulation value	K	818.3	818.3	800.2	698.4
		Relative error	%	**0.11**	**0.11**	**0.13**	**0.23**
	$T_{EX,G}$	Design value	K	385.6	379.0	373.0	377.4
		Simulation value	K	382.3	374.8	368.8	372.0
		Relative error	%	**0.84**	**1.08**	**1.11**	**1.43**
	$p_{LS,HP}$	Design value	MPa	12.035	10.021	8.272	5.397
		Simulation value	MPa	11.988	9.974	8.208	5.349
		Relative error	%	**0.39**	**0.47**	**0.77**	**0.88**
	$p_{LS,IP}$	Design value	MPa	3.051	2.517	2.052	1.478
		Simulation value	MPa	3.074	2.535	2.076	1.495
		Relative error	%	**0.74**	**0.71**	**1.18**	**1.16**
	$p_{LS,LP}$	Design value	MPa	2.362E-01	2.021E-01	1.683E-01	1.623E-01
		Simulation value	MPa	2.383E-01	2.005E-01	1.702E-01	1.647E-01
		Relative error	%	**0.89**	**0.79**	**1.13**	**1.48**
	P_{ST}	Design value	MW	74.83	59.52	46.45	27.95
		Simulation value	MW	74.39	59.19	46.17	27.78
		Relative error	%	**0.59**	**0.55**	**0.60**	**0.61**
	η_{CC}	Design value	%	79.71	77.55	73.62	60.77
		Simulation value	%	79.63	77.47	73.54	60.70
		Relative error	%	**0.10**	**0.10**	**0.11**	**0.12**

Table S4

Comparison between simulation results and design data (provided by the manufacturer) of 2×1 plant at various conditions.

Item			Unit	PF_{GT} = 100%	PF_{GT} = 75%	PF_{GT} = 50%	PF_{GT} = 30%
Boundary conditions	T_A		K	269.0	269.0	269.0	269.0
	P_{GT}		MW	297.67	223.22	148.80	89.28
	Q		GJ/h	1667.45	1246.63	1013.17	662.01
	p_{CD}		kPa	3.6	3.6	3.6	3.6
	$T_{IN,G}$	Design value	K	817.5	817.5	801.3	700.1

		Simulation value	K	818.3	818.3	800.2	698.4
		Relative error	%	**0.11**	**0.11**	**0.13**	**0.23**
	$T_{EX,G}$	Design value	K	385.4	379.9	374.5	380.1
		Simulation value	K	382.9	375.8	369.6	373.1
		Relative error	%	**0.64**	**1.06**	**1.29**	**1.84**
	$p_{LS,HP}$	Design value	MPa	12.419	10.368	8.519	5.557
		Simulation value	MPa	12.377	10.281	8.448	5.501
		Relative error	%	**0.34**	**0.84**	**0.83**	**1.01**
	$p_{LS,IP}$	Design value	MPa	3.230	2.667	2.136	1.572
Validation		Simulation value	MPa	3.206	2.642	2.161	1.554
parameters		Relative error	%	**0.73**	**0.95**	**1.18**	**1.13**
	$p_{LS,LP}$	Design value	MPa	3.128E-01	2.725E-01	2.241E-01	2.183E-01
		Simulation value	MPa	3.168E-01	2.752E-01	2.219E-01	2.162E-01
		Relative error	%	**1.28**	**0.99**	**0.98**	**0.96**
	P_{ST}	Design value	MW	152.78	124.81	93.25	56.53
		Simulation value	MW	152.13	124.24	93.83	56.94
		Relative error	%	**0.43**	**0.46**	**0.62**	**0.72**
	η_{CC}	Design value	%	80.45	78.38	74.37	60.98
		Simulation value	%	80.34	78.27	74.49	61.09
		Relative error	%	**0.14**	**0.14**	**0.16**	**0.18**

1

S2. Difference in fuel consumption of each demand in 7 calculation cases

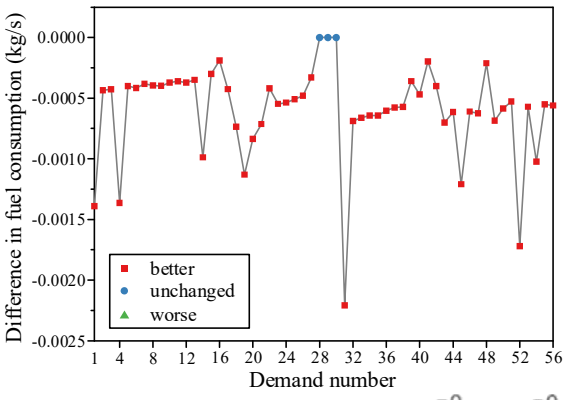

(a) Case1: R_H increases from $0.6R_H^O$ to $0.8R_H^O$

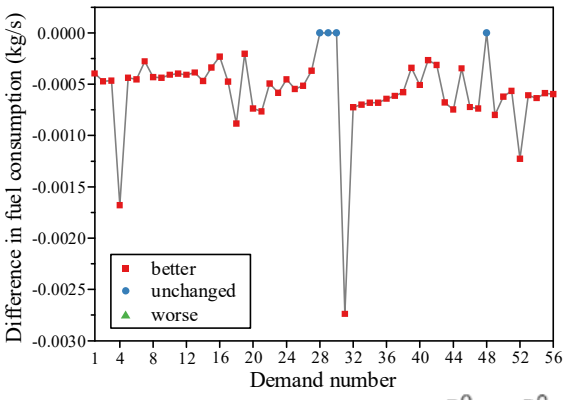

(b) Case2: R_H increases from $0.8R_H^O$ to $1R_H^O$

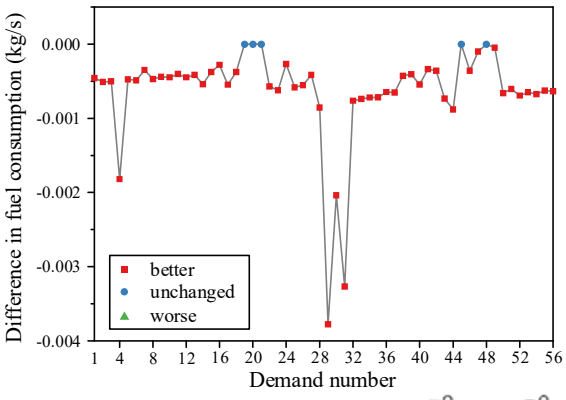

(c) Case3: R_H increases from $1R_H^O$ to $1.2R_H^O$

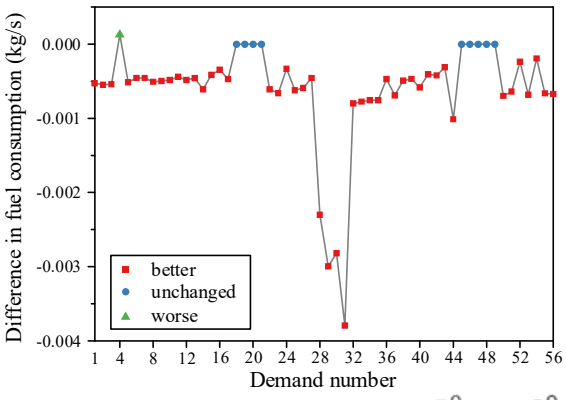

(d) Case4: R_H increases from $1.2R_H^O$ to $1.4R_H^O$

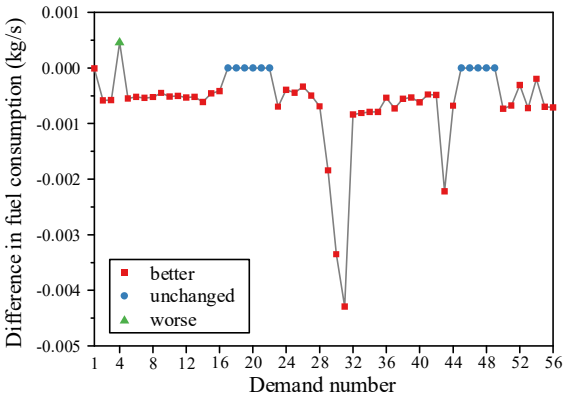

(e) Case5: R_H increases from $1.4R_H^O$ to $1.6R_H^O$

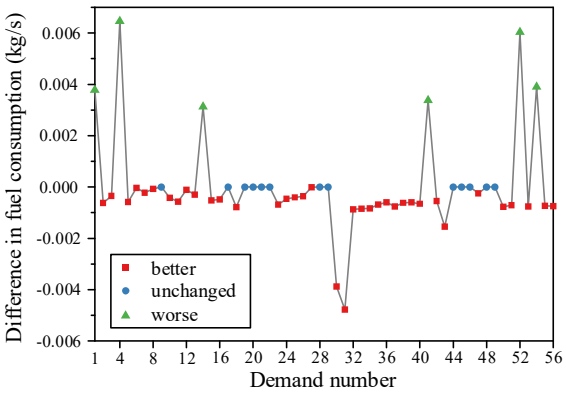

(f) Case6: R_H increases from $1.6R_H^O$ to $1.8R_H^O$

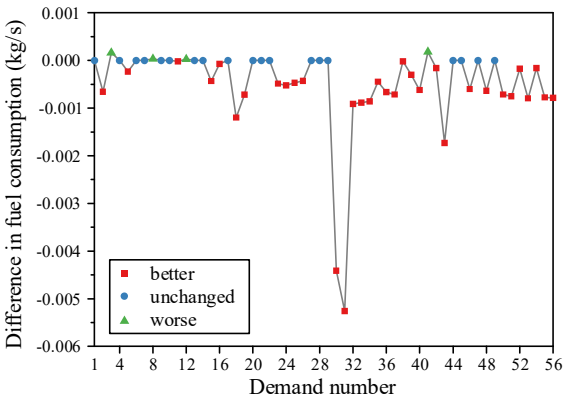

(g) Case7: R_H increases from $1.8R_H^O$ to $2R_H^O$

Fig. S3. Difference in fuel consumption of each demand in 7 calculation cases.

S5. Changes in economic performance of the CHPED results of the demands at each state

Table S5

Changes in economic performance of the CHPED results of the demands at each state.

State	Total amount	Changes in economic performance of the CHPED results after the decrease of R_H		
		Better	Unchanged	Worse
State1	223	1	0	222
State2	47	0	0	47
State3	70	11	27	32
State4	52	0	37	15